Deep-Sea Research II 56 (2009) 2503–2519

Contents lists available at ScienceDirect

Deep-Sea Research II

journal homepage: www.elsevier.com/locate/dsr2

Modeling iron limitation of primary production in the coastal Gulf of Alaska

Jerome Fiechter [a,*], Andrew M. Moore [a], Christopher A. Edwards [a], Kenneth W. Bruland [a], Emanuele Di Lorenzo [b], Craig V.W. Lewis [c], Thomas M. Powell [d], Enrique N. Curchitser [e], Kate Hedstrom [f]

[a] Department of Ocean Sciences, University of California, Santa Cruz, USA
[b] School of Earth and Atmospheric Sciences, Georgia Institute of Technology, Georgia, USA
[c] NATO Undersea Research Center, La Spezia, Italy
[d] Department of Integrative Biology, University of California, Berkeley, USA
[e] Institute of Marine and Coastal Sciences, Rutgers University, New Jersey, USA
[f] Arctic Region Supercomputing Center, Fairbanks, Alaska, USA

ARTICLE INFO

Article history:
Accepted 27 February 2009
Available online 25 March 2009

Keywords:
Ecosystems
Models
Iron
Limiting factors
Phytoplankton
Variability

ABSTRACT

A lower trophic level NPZD ecosystem model with explicit iron limitation on nutrient uptake is coupled to a three-dimensional coastal ocean circulation model to investigate the regional ecosystem dynamics of the northwestern coastal Gulf of Alaska (CGOA). Iron limitation is included in the NPZD model by adding governing equations for two micro-nutrient compartments: dissolved iron and phytoplankton-associated iron. The model has separate budgets for nitrate (the limiting macro-nutrient in the standard NPZD model) and for iron, with iron limitation on nitrate uptake being imposed as a function of the local phytoplankton realized Fe:C ratio. While the ecosystem model represents a simple approximation of the complex lower trophic level ecosystem of the northwestern CGOA, simulated chlorophyll concentrations reproduce the main characteristics of the spring bloom, high shelf primary production, and "high-nutrient, low-chlorophyll" (HNLC) environment offshore. Over the 1998–2004 period, model-data correlations based on spatially averaged, monthly mean chlorophyll concentrations are on average 0.7, with values as high as 0.9 and as low as 0.5 for individual years. The model also provides insight on the importance of micro- and macro-nutrient limitation on the shelf and offshore, with the shelfbreak region acting as a transition zone where both nitrate and iron availability significantly impact phytoplankton growth. Overall, the relative simplicity of the ecosystem model provides a useful platform to perform long-term simulations to investigate the seasonal and interannual CGOA ecosystem variability, as well as to conduct sensitivity studies to evaluate the robustness of simulated fields to ecosystem model parameterization and forcing. The ability of the model to differentiate between nitrate-limited, and iron-limited growth conditions, and to identify their spatial and temporal occurrences, is also a first step towards understanding the role of environmental gradients in shaping the complex CGOA phytoplankton community structure.

1. Introduction

The importance of the rich and diverse marine resources of the coastal Gulf of Alaska (CGOA) has been recognized by the U.S. GLOBEC (Global Ocean Ecosystem Dynamics) program and, thus, the region is designated as a study site to investigate the potential impact of global climate change on ecosystem dynamics and fisheries. Of particular interest is the northwestern CGOA (from ca. 142° to 162° W, along the Alaskan Peninsula) (Fig. 1, left), where the shelf region undergoes significant physical and biological variability on monthly, seasonal, and interannual timescales due to the different oceanographic processes impacting the region. The inner-shelf circulation is associated with the Alaska Coastal Current (ACC), which is locally forced by along-shore winds and buoyancy from freshwater discharge (Royer, 1981). In contrast, the outer-shelf circulation is dominated by the Alaskan Stream, which is the western boundary current associated with the eastern Pacific subarctic gyre (Reed, 1984). The mesoscale variability along the northwestern CGOA shelfbreak is also seasonally modulated by southwestward propagating eddies, which have been observed to significantly modulate cross-shelf exchange of physical and biological properties (Okkonen et al., 2003).

The relatively high level of primary production associated with the northwestern CGOA ecosystem is somewhat unexpected considering that the atmospheric wind forcing in the region is predominantly downwelling-favorable, implying that subsurface

* Corresponding author. Tel.: +1 831 459 3924; fax: +1 831 459 4882.
E-mail address: fiechter@ucsc.edu (J. Fiechter).

0967-0645/$ - see front matter © 2009 Elsevier Ltd. All rights reserved.
doi:10.1016/j.dsr2.2009.02.010

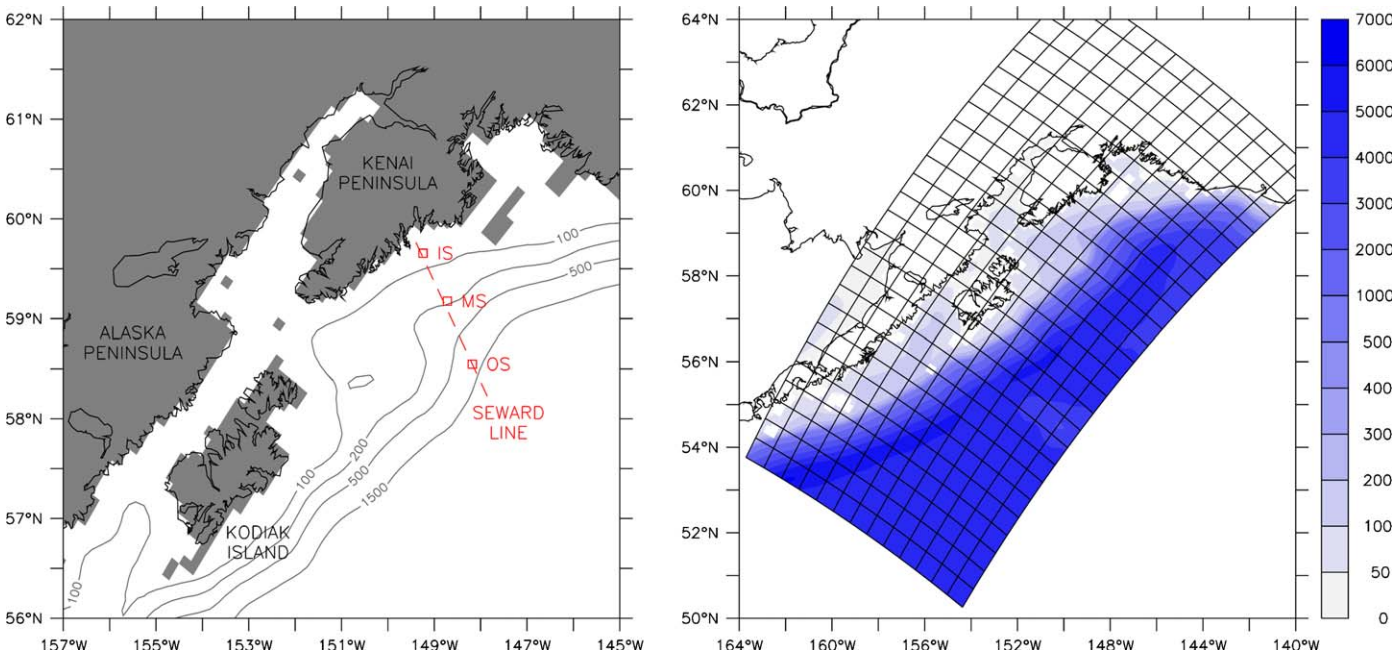

Fig. 1. Geographical maps of northwestern CGOA with in situ observations and model domain. Left: locations of GLOBEC observations (Seward line, inner- (IS), mid- (MS), and outer-shelf (OS) stations); contour lines indicate bottom topography (m). Right: model grid (subsampled by a factor of 5 for clarity) and bottom topography (m).

nutrients are not readily upwelled onto the continental shelf (as is the case, for instance, along the west coast of the United States). Consequently, other cross-shelf transport mechanisms must be invoked to explain nutrient replenishment of the shelf waters. Observational evidence suggests that onshore transport of macro-nutrients (e.g., nitrate) occurs through a wide range of physical processes; such as surface Ekman transport, eddies, topographic steering, tidal mixing, and relaxation of downwelling conditions (Stabeno et al., 2004; Ladd et al., 2005). In contrast, micro-nutrients (e.g., iron) are typically supplied to coastal waters from river discharge and sediment resuspension on the shelf (Stabeno et al., 2004). Since the two major limiting nutrients in the region are nitrate and iron, their cross-shelf concentration gradients, and modulation by environmental factors, significantly shape the phytoplankton community structure of the northwestern CGOA (Martin and Fitzwater, 1988; Strom et al., 2006). Offshore transport of iron-rich shelf waters by mesoscale eddies (Whitney et al., 2005) or by entrainment along the equatorward edge of the subarctic gyre (Lam et al., 2006) also can result in enhanced primary production in the "high-nutrient, low-chlorophyll" (HNLC) environment of the Gulf of Alaska basin by alleviating iron limitation on phytoplankton growth.

Varying degrees of complexity have been used to explore the sensitivity of phytoplankton growth to iron availability in lower trophic level ecosystem models. In a first class of models, iron limitation effects on phytoplankton uptake of macro-nutrients are introduced directly through a growth reduction constant (Denman and Peña, 1999; Denman et al., 2006), or indirectly through changes in light limitation and silicate half-saturation parameters (Chai et al., 2002; Jiang and Chai, 2004; Fujii et al., 2005). Alternatively, other models include dissolved iron explicitly as a state variable, generally limiting micro-nutrient uptake as a Michaelis–Menten function of dissolved iron concentrations (Leonard et al., 1999; Archer and Johnson, 2000; Moore et al., 2002; Aumont et al., 2003; Gregg et al., 2003). In these models, iron concentrations vary through biological uptake and recycling, relaxation of deep concentrations to observed values, as well as through physical fluxes due to oceanic transport and aeolian deposition at the surface of the ocean. Although a wide range of coupled physical-biological models of varying complexity have been developed for coastal regions of the eastern Pacific (Wroblewski, 1977; Franks et al., 1986; Spitz et al., 2003; Powell et al., 2006), only one other has attempted to specifically address the role of iron limitation on phytoplankton growth in the CGOA (Hinckley et al., 2009).

The objective of the present study is to investigate the regional ecosystem dynamics of the northwestern CGOA using an NPZD lower trophic level ecosystem model with explicit iron limitation, coupled to a three-dimensional coastal ocean circulation model. The relative simplicity (i.e. six components) of the ecosystem model and low horizontal resolution (i.e. 10 km) of the ocean circulation model provide an ideal configuration to perform long-term simulations (i.e. 10 years) and sensitivity studies. The model results are thus useful to study the CGOA ecosystem variability on timescales ranging from seasonal to interannual, as well as to evaluate the robustness of the simulated fields to ecosystem model parameterization and surface forcing. More specifically, model-data comparisons with available remotely sensed and in situ observations are performed to evaluate the ability of the model to reproduce the cross-shelf and vertical structure of nitrate, iron and chlorophyll concentrations, as well as their temporal variability.

2. Ocean circulation model (ROMS)

The ocean circulation model for the northwestern CGOA is an implementation of the Regional Oceanic Modeling System (ROMS) (Haidvogel et al., 2000; Shchepetkin and McWilliams, 2005). ROMS is a hydrostatic, primitive equation model that uses terrain-following vertical coordinates and a split-mode technique to solve efficiently for internal (i.e. depth-dependent) and external (i.e. depth-integrated) variables. The oceanic surface boundary layer is computed with a non-local, K-profile parameterization (KPP) (Large et al., 1994). The model grid for the CGOA has a horizontal resolution of 10 km (130 × 66 nodes) and 42 non-uniform vertical

levels, with clustering near the surface (Fig. 1, right). The source for the bottom topography mapped on the CGOA grid is based upon ETOPO 5 with manual corrections in Shelikof Strait, and the minimum water depth is set to 30 m. The bottom topography is also smoothed to reduce pressure gradient errors due to the terrain-following vertical coordinate. At 10 km horizontal resolution, the model grid may not fully resolve fine-scale flow-topography interactions or ACC frontal dynamics on the inner-shelf, but it is eddy-permitting offshore and, thus, should adequately capture mesoscale variability at the shelfbreak. In fact, a similar horizontal grid resolution (i.e. 14–20 km) of the order of the Rossby radius of deformation has been used previously to study the intrinsic mesoscale variability of the Alaskan Stream in the northwestern CGOA (Combes and Di Lorenzo, 2007). Finally, the internal (baroclinic) time step for the CGOA model is 600 s, and the model is integrated in time for a period of 10 years from 1995 through 2004.

The ROMS ocean circulation model for the CGOA is driven on all open boundaries by monthly averaged sea-surface height, velocity, temperature and salinity fields from the Northeast Pacific (NEP) ROMS simulations of Curchitser et al. (2005) at the same horizontal and vertical resolution (i.e. one-way offline nesting). This approach allows specifying realistic transport values and temperature and salinity profiles for the Alaskan Stream entering and exiting the CGOA domain near 59°N, 142°W and 54°N, 162°W, respectively. The NEP model extends from approximately 20°N to 71°N and uses a coupled ocean/sea ice version of ROMS (Budgell, 2005) for the integration from 1958 through 2004. The surface forcing for the NEP model is derived from the data sets for Common Ocean-Ice Reference Experiments (CORE; Large and Yeager, 2004), which consists of 6-hourly winds, air temperatures, sea-level pressure, specific humidity, and daily short-wave and downwelling long-wave radiation. Precipitation is derived from montly mean values, and riverine inputs are implemented as a distributed line source of fresh water in the Gulf of Alaska (Royer, 1998). The Columbia, Yukon, and Copper Rivers are explicitly added as point sources using data from the US Geological Survey data sets (http://nwis.waterdata.usgs.gov/nwis). The surface forcing for the CGOA model is derived from the momentum, heat, and salt fluxes computed in the NEP model, and is in the form of monthly averaged wind stress, freshwater (E-P) flux, net heat flux, and short-wave radiation. Open boundary conditions and surface forcing are linearly interpolated at each time step between the monthly averaged values to guarantee smooth variations in time. The sensitivity of simulated chlorophyll concentrations to the temporal resolution of surface and open boundary forcing is investigated by running the model for 1 year (2001) with daily and weekly averaged forcing fields, and comparing to the results with monthly averaged forcing fields (see Results section).

3. Ecosystem trophic level model with iron limitation

3.1. NPZD model

A simple four-component NPZD model (Powell et al., 2006) is used to express the basic ecological processes in the pelagic region of the CGOA. In the model, the four components (dissolved nitrogen concentration (N); phytoplankton biomass (P), zooplankton biomass (Z); and detritus (D)) are expressed in terms of nitrogen concentrations. The processes incorporated in the governing equations (Table 1) include autotrophic growth of phytoplankton controlled by light and a single macro-nutrient (nitrate). The addition of iron limitation to phytoplankton growth is described separately in Section 3.2, as it is a significant addition to previous implementations of this simple NPZD model. Uptake of nitrogen by phytoplankton during the growth process is represented via a Michaelis–Menten formulation; and grazing by zooplankton upon phytoplankton with an Ivlev formulation. The model also allows for inefficient grazing by zooplankton upon phytoplankton through a "feeding efficiency" constant. Natural loss processes (i.e. mortality) for both phytoplankton and zooplankton are linear in P and Z, and remineralization of detritus is also linear in D. Values for the parameters of the NPZD model are listed in Table 2.

One-way coupling to the CGOA ocean circulation model is achieved by solving a transport equation in ROMS at every time step for each ecosystem model component. Sinking of detritus is

Table 1
Biological source and sink terms for the NPZD model, and growth functions for phytoplankton and zooplankton (see Table 2 for parameter definitions and values).

NPZD lower trophic level ecosystem model

Nitrate:

$$\frac{\partial N}{\partial t} = \delta D + \gamma_n GZ - UP$$

Phytoplankton:

$$\frac{\partial P}{\partial t} = UP - GZ - \sigma_d P$$

Zooplankton:

$$\frac{\partial Z}{\partial t} = (1-\gamma_n)GZ - \zeta_d Z$$

Detritus:

$$\frac{\partial D}{\partial t} = \sigma_d P + \zeta_d Z - \delta D + w_d \frac{\partial D}{\partial z}$$

Light availability at depth (negative z):

$$I = I_0 \exp\left(k_z z + k_p \int_z^0 P(z')dz'\right)$$

Nitrate-limited phytop. growth rate:

$$U_N = \frac{V_m N}{N + k_N} \frac{\alpha I}{\sqrt{V_m^2 + \alpha^2 I^2}}$$

Zooplankton growth rate:

$$G = R_m(1 - e^{-\Lambda P})$$

Table 2
Parameter names, symbols, values, and units for the NPZD model.

Parameter name	Symbol	Value	Units
Light extinction coefficient	k_z	0.067	m^{-1}
Self-shading coefficient	k_p	0.04	$m^2\,mmolN^{-1}$
Initial slope of P-I curve	α	0.02	$m^2\,W^{-1}$
Phytop. nitrate uptake rate	V_m	1.0	day^{-1}
Nitrate half-saturation coeff.	k_N	1.0	$mmolN\,m^{-3}$
Phytop. senescence	σ_d	0.1	day^{-1}
Zoop. grazing rate	R_m	0.65	day^{-1}
Ivlev constant	Λ	0.84	–
Zoop. excretion efficiency	γ_n	0.3	–
Zoop. mortality	ζ_d	0.145	day^{-1}
Detritus remineralization	δ	1.0	day^{-1}
Detritus sinking	w_d	8.0	$m\,day^{-1}$

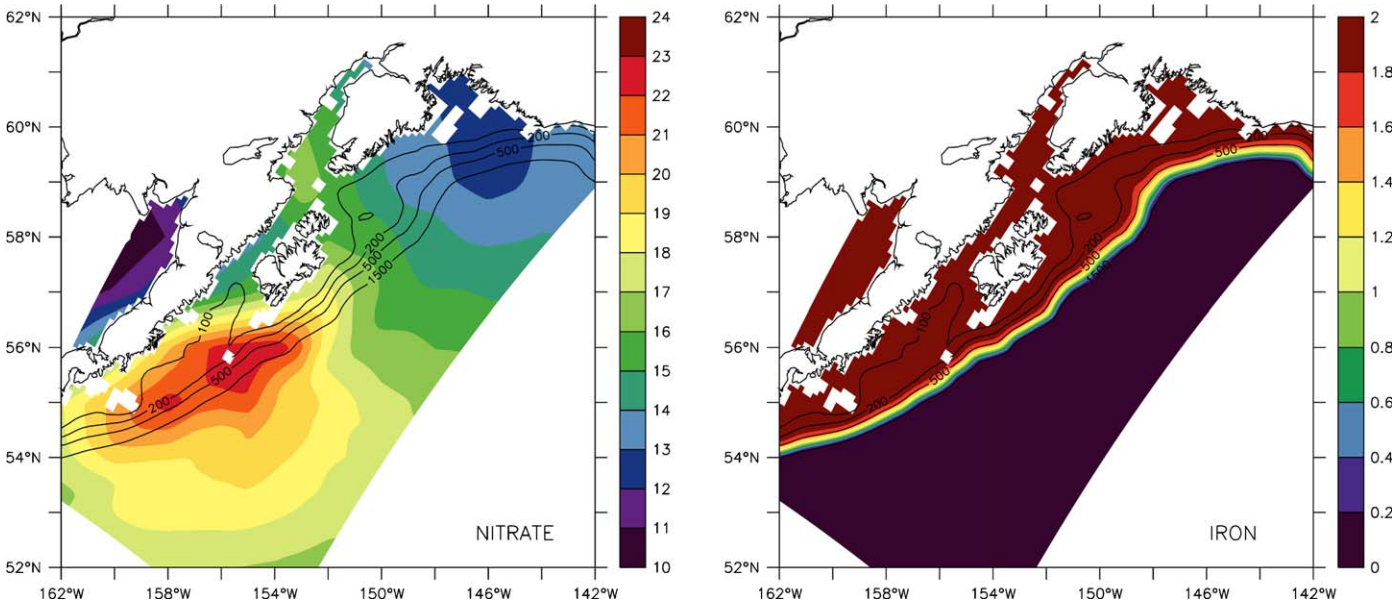

Fig. 2. Initial conditions for surface nitrate concentration (mmolN m^{-3}) (left) and dissolved iron concentration (μmol m^{-3}) (right). Contour lines indicate bottom topography (m).

represented by a vertical velocity proportional to the product of a constant sinking velocity and the local vertical detritus concentration gradient. All biological source and sink terms (e.g., phytoplankton growth, zooplankton grazing) are also computed at every ROMS time step. Initial and boundary conditions for nitrate are derived from monthly climatological concentrations (World Ocean Atlas 2001, $1^\circ \times 1^\circ$ horizontal resolution (Conkright and Boyer, 2002)) (Fig. 2, left). For lack of better information, initial and boundary conditions for phytoplankton, zooplankton, and detritus are set to a small value (0.01 mmolN m^{-3}).

3.2. Iron limitation model

The approach to modeling iron limitation used in the present study reflects an awareness that iron uptake by phytoplankton is not simply a function of available, dissolved concentrations, nor does it occur simply in proportion to macronutrient uptake and loss. Laboratory measurements demonstrated for a range of coastal and oceanic algal groups that cellular iron to carbon ratios are not constant and can, under iron-rich conditions, reach 30 times that needed for maximum growth (Sunda and Huntsman, 1995). The potential for cells to absorb and store excess iron when in nutrient-replete conditions has potential impact for survival in environments characterized by episodic or intermittent nutrient input. While the implications of this luxury iron uptake have been specifically discussed for both the California Current and Peru upwelling systems (Bruland et al., 2001, 2005), it is reasonable to assume that modeling this capability is appropriate in other regions as well.

By treating iron limitation on phytoplankton growth explicitly, the model represents an improvement over earlier models for the subarctic northeast Pacific region, which included iron limitation implicitly through a phytoplankton growth reduction constant fitted to reproduce a "normal" annual cycle (Denman and Peña, 1999; Denman et al., 2006). Iron limitation on phytoplankton growth is included explicitly through Michaelis–Menten kinetics, and in that regard, the model described here is comparable to other ecosystem models with iron limitation developed for the global ocean (Archer and Johnson, 2000; Moore et al., 2002; Aumont et al., 2003). However, in the present formulation, the Michaelis–Menten kinetics for iron limitation is based on the local phytoplankton realized Fe:C ratio, as opposed to the local dissolved iron concentration. This approach has the advantage of having a spatially and temporally varying Fe:C ratio calculated directly from the local dissolved iron and phytoplankton concentrations, instead of treating the Fe:C ratio as constant (Leonard et al., 1999; Archer and Johnson, 2000) or parameterized based on iron- and light-limitation terms (Aumont et al., 2003). In addition, with the local Fe:C ratio computed explicitly in the model, iron uptake can be defined as a function of the phytoplankton empirical and realized Fe:C ratios, thus allowing for "luxury" iron uptake by phytoplankton (a biological process not represented in even the more complex global ecosystem models with iron limitation; e.g., Moore et al., 2002). Like most other ecosystem models with iron limitation, the present formulation assumes that all dissolved iron is readily available for phytoplankton uptake, regardless of metabolic effects associated with iron speciation (Shaked et al., 2005).

The implementation of the iron limitation model only requires modification of the equation for phytoplankton growth in the NPZD model, as well as the addition of governing equations for two more nutrient compartments: dissolved iron, F_d, and bioavailable iron already incorporated within phytoplankton cells, F_p (Table 3). Hence, the model involves separate budgets for nitrate (the limiting nutrient in the standard NPZD model) and for iron. Dissolved iron is incorporated into phytoplankton cells through a relaxation to empirically determined levels that depend as a power law on the local dissolved iron concentration. Only a fraction (f_{rem}) of phytoplankton-associated iron is returned to the dissolved compartment as a result of phytoplankton mortality and grazing, with the remainder assumed to be instantly exported from the system. Iron limitation is imposed through a Michaelis–Menten function of the phytoplankton realized Fe:C ratio. The parameter values for Fe:C as a function of dissolved iron concentration and for iron limitation on phytoplankton growth are derived from existing in situ observations and laboratory experiments (Sunda and Huntsman, 1995). Both empirically determined (R_0) and realized (R) Fe:C ratio vary spatially and temporally, as they depend on the local dissolved iron, phytoplankton-associated iron, and phytoplankton concentrations. The realized Fe:C ratio is computed by converting the phytoplankton-equivalent nitrogen concentrations (mmolN m^{-3})

to carbon concentrations (mmolC m^{-3}) using a constant C:N Redfield ratio of 106:16 molC $molN^{-1}$. Parameters values for the iron limitation model are listed in Table 4.

One-way coupling to the CGOA ocean circulation model is achieved by solving a transport equation in ROMS at every time step for each component of the iron limitation model. All biological source and sink terms (e.g., phytoplankton uptake) for iron concentrations are also updated at every ROMS time step in conjunction with the NPZD model. The initial and boundary conditions for dissolved iron are based on observed concentrations for the Gulf of Alaska (Martin et al., 1989) and have been set to vary from 2.0 μmolFe m^{-3} inshore of the 200 m isobath to 0.05 μmolFe m^{-3} offshore of the 1500 m isobath, with a linear transition in between (Hinckley et al., 2009) (Fig. 2, right). To simulate iron replenishment from river discharge and sediment resuspension, the dissolved iron concentrations on the inner-shelf (i.e. inshore of the 200 m isobath) in the model are relaxed to the observed value (i.e. 2.0 μmolFe m^{-3}) on a 5-day timescale.

3.3. Ecosystem model parameterization

While most of the NPZD parameters were kept at their default values (Powell et al., 2006), two were modified. First, the light attenuation coefficient associated with phytoplankton self-shading was increased from 0.0095 to 0.04 m^2 $mmolN^{-1}$ to match previously used values for the north Pacific (Kishi et al., 2007). The increase in phytoplankton self-shading was necessary to reproduce vertical chlorophyll profiles on the inner-shelf during the spring bloom (i.e. when chlorophyll concentrations are largest). The value used for light attenuation due to sea water (i.e. 0.067 m^{-1}) represents an average between clear oceanic water (typically 0.04 m^{-1}; e.g., Lima et al., 2002) and more turbid shelf waters (0.1 m^{-1} or larger; e.g.,Hofmann, 1988). Decreasing the light attenuation coefficient to an oceanic water value does not significantly impact simulated chlorophyll concentrations in the basin, as phytoplankton growth in that region is predominantly limited by dissolved iron availability. Second, the zooplankton grazing rate was increased to match in situ observations from the CGOA which indicate that microzooplankton consume all of the small ($<20\,\mu m$) phytoplankton and nearly half of the large ($>20\,\mu m$) phytoplankton production (Strom et al., 2007). The sensitivity of simulated chlorophyll concentrations to a few important biological processes is investigated by running the model for 1 year (2001) with different parameter values for the zooplankton grazing rate, detritus remineralization rate, and phytoplankton Fe:C half-saturation constant (see Results section).

Table 3
Biological source and sink terms for the iron limitation model, and dissolved iron climatology (see Table 4 for parameter definitions and values).

Iron limitation model
P-associated iron:

$$\frac{\partial F_p}{\partial t} = F_p\left(U - \frac{GZ}{P} - \sigma_d\right) + L_{\mathrm{Fe}}$$

Dissolved iron:

$$\frac{\partial F_d}{\partial t} = F_p\left(f_{rem}\left(\frac{GZ}{P} + \sigma_d\right) - U\right) - L_{\mathrm{Fe}}$$

Iron uptake by phytoplankton:

$$L_{\mathrm{Fe}} = \frac{R_0 - R}{t_{\mathrm{Fe}}} P[\mathrm{C:N}]$$

Empirically determined and realized [Fe:C] ratios:

$$R_0 = bF_d^a, \quad R = \frac{F_p}{P[\mathrm{C:N}]}$$

Iron limitation on phytoplankton growth:

$$U = min(R^2/(R^2 + k^2), U_N)$$

U_N: nitrate-limited phytoplankton growth rate
[C:N] = 106:16 molC $molN^{-1}$: Redfield carbon-to-nitrogen ratio

Dissolved iron climatology

$$F_{d,c\,\mathrm{lim}} = F_{d,\max} + c_{\mathrm{Fe}}(F_{d,\min} - F_{d,\max}), \quad c_{\mathrm{Fe}} = \max\left(0, \min\left(1, \frac{h - h_{\min}}{h_{\max} - h_{\min}}\right)\right)$$

Table 4
Parameter names, symbols, values, and units for the iron limitation model and dissolved iron climatology.

Parameter name	Symbol	Value	Units
Iron limitation model			
Iron uptake time scale	t_{Fe}	1.0	Day
Empirical [Fe:C] power	a	0.6	–
Empirical [Fe:C] coefficient	b	64	$(molC\,m^{-3})^{-1}$
Half-saturation [Fe:C]	k_{Fe}	16.9	μmolFe $(molC)^{-1}$
Iron remineralization fraction	f_{rem}	0.5	–
Dissolved iron climatology			
Min. dissolved iron	$F_{d,min}$	0.05	μmolFe m^{-3}
Max. dissolved iron	$F_{d,max}$	2.0	μmolFe m^{-3}
Inshore transition depth	h_{min}	200	m
Offshore transition depth	h_{max}	1500	m

4. Results

The results from the coupled physical–biological model are extracted from the 10-year simulation (1995 through 2004) in the form of monthly means for the years 1998 through 2004. The model fields thus include a 3-year spin-up, which allows for the physical and biological seasonal cycles to fully establish. The results also cover the first 6 years for which ocean color satellite imagery (SeaWiFS) is available for comparison.

4.1. Interannual variability (1998–2004)

To evaluate the ability of the model to reproduce the dominant spatial and temporal patterns present in the observations (e.g., timing of spring bloom, shelf production vs. offshore HNLC), observed and simulated chlorophyll concentrations are compared in a "climatological" sense based on monthly means/composite images for each month over the 7-year period. Simulated chlorophyll concentrations are obtained by multiplying simulated phytoplankton nitrogen concentrations by a Chl:N ratio of 1.325 gChl $molN^{-1}$ (derived from a C:N Redfield ratio of 106:16 molC $molN^{-1}$ and a C:Chl ratio of 60:1 gC $gChl^{-1}$). Since winter production in the CGOA is severely limited by low light conditions, the seasonal variability in simulated and observed chlorophyll concentrations is presented for spring, summer, and fall phytoplankton growth conditions (Fig. 3). As expected, the largest chlorophyll concentrations (5–10 mg m^{-3}) in the model and observations occur during the spring bloom (i.e. May) and are mainly confined to the CGOA shelf (i.e. inshore of the 1500 m isobath). On average, the model overestimates surface chlorophyll concentrations by a factor of two, and underestimates the width of the transition region between high and low chlorophyll environments at the shelfbreak. During summer (i.e. July) and fall (i.e. September), the model still predicts distinct

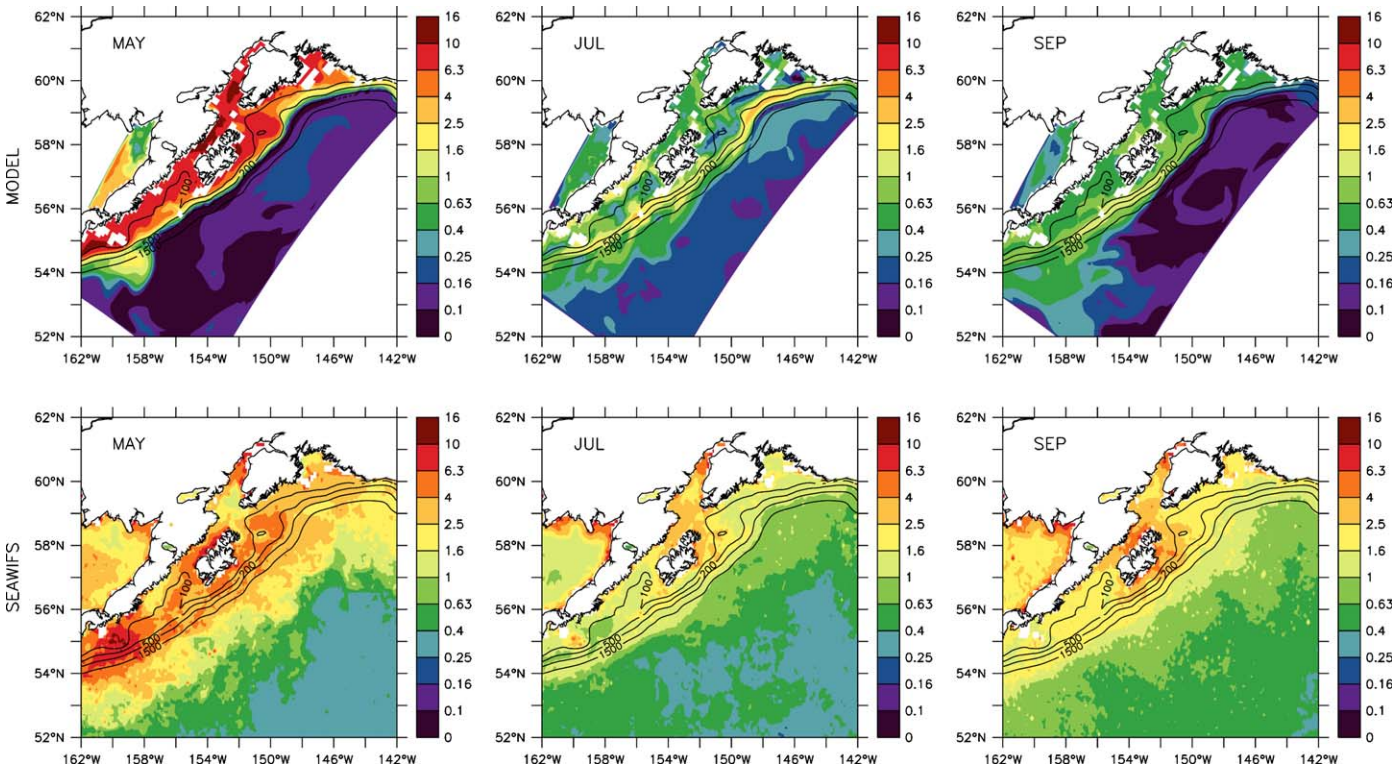

Fig. 3. Monthly "climatology" for 1998–2004 simulated (upper) and observed (SeaWiFS) (lower) surface chlorophyll concentrations (mg m^{-3}) for May (left), July (center), and September (right). Contour lines indicate bottom topography (m). Source for SeaWiFS data: NOAA CoastWatch Program (http://coastwatch.pfel.noaa.gov).

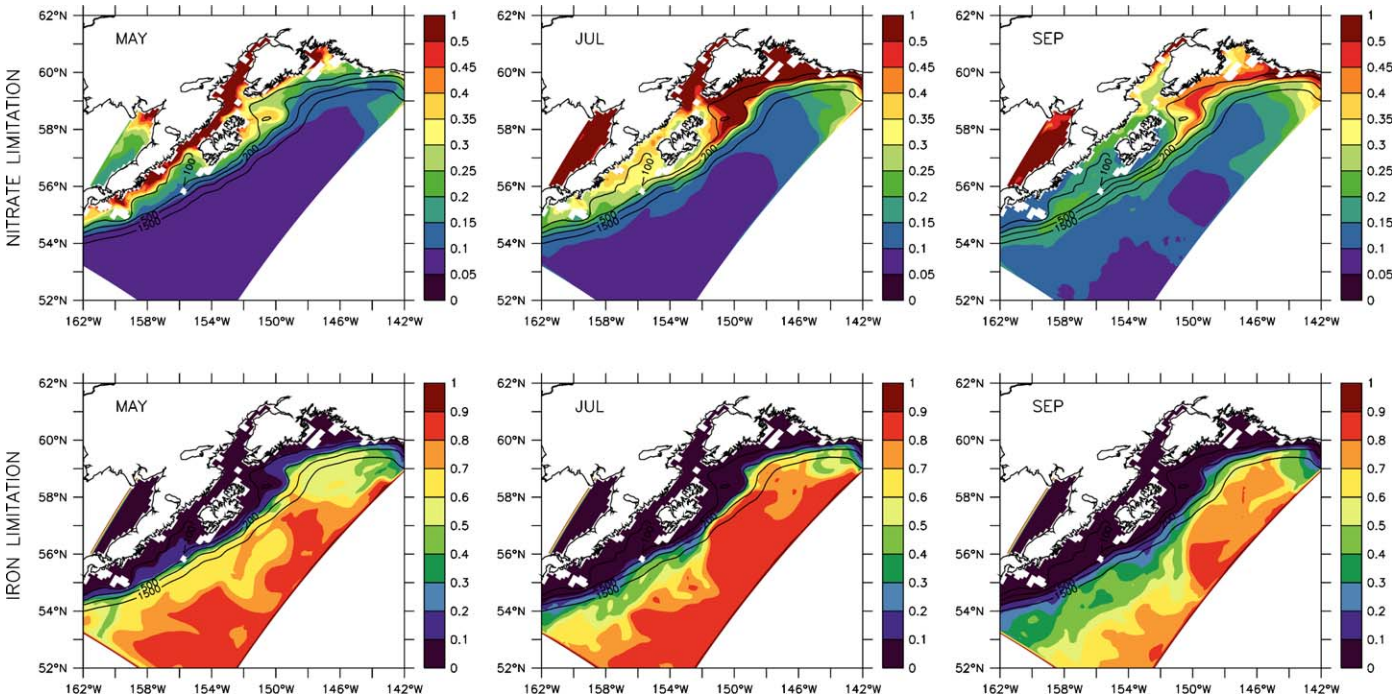

Fig. 4. Monthly "climatology" for 1998–2004 simulated phytoplankton growth limitation factor (non-dimensional) by nitrate ($(1-N/(N+k_N))$; upper) and iron ($(1-R^2/(R^2+k_{Fe}^2))$; lower) for May (left), July (center), and September (right). A value of zero indicates no growth limitation and a value of one indicates 100% growth limitation. Contour lines indicate bottom topography (m).

phytoplankton growth regimes on the shelf and offshore, but underestimates chlorophyll concentrations on the shelf by a factor of roughly five (i.e. 0.5–1.0 mg m^{-3} vs. 1.5–4 mg m^{-3} on average).

Since the model is able to distinguish between the high production region on the shelf and HNLC region offshore, computing similar "climatological" means for nitrate and iron limitation on phytoplankton growth is useful to investigate the contribution of each nutrient to the spatial and temporal ecosystem variability (Fig. 4). As expected, the growth limitation factors, defined as $(1-N/(N+K_N))$ and $(1-R^2/(R^2+k_{Fe}^2))$, indicate that nitrate is the limiting nutrient on the shelf, and iron is the limiting nutrient offshore (i.e. a value of zero for the growth limitation

factors represents no limitation, and a value of one represents 100% limitation). The overall phytoplankton growth reduction by nitrate on the shelf ranges on average between 20% and 40% during spring and fall, and between 30% and 60% during summer when nutrient drawdown is largest. While nitrate limitation is spatially uniform during spring (except for large values directly near the coast), phytoplankton growth reduction during summer and fall is ca. 50% more severe on the northern CGOA shelf than on the southwestern CGOA shelf, with the transition region located roughly between the Kenai Peninsula and Kodiak Island. The overall phytoplankton growth reduction by iron in the basin ranges on average between 60% and 80%, with slightly higher values in summer (up to 90%), and slightly lower values in fall (down to 40%). Changes in iron limitation are predominantly in the cross-shelf direction and exhibit significant temporal variability in the shelfbreak region, which alludes to the importance of dissolved iron availability in shaping the CGOA cross-shelf phytoplankton community structure. While the model generally predicts correct spatial nutrient limitation patterns (as currently understood), the overly narrow transition region between the high and low chlorophyll environments suggests that the "climatology" used to set the initial conditions for the dissolved iron cross-shelf gradient may be too restrictive at the shelfbreak.

The ability of the model to reproduce the observed interannual variability during 1998–2004 is first assessed qualitatively by comparing spatially averaged, monthly mean simulated and remotely sensed (SeaWiFS) chlorophyll concentration. Since the

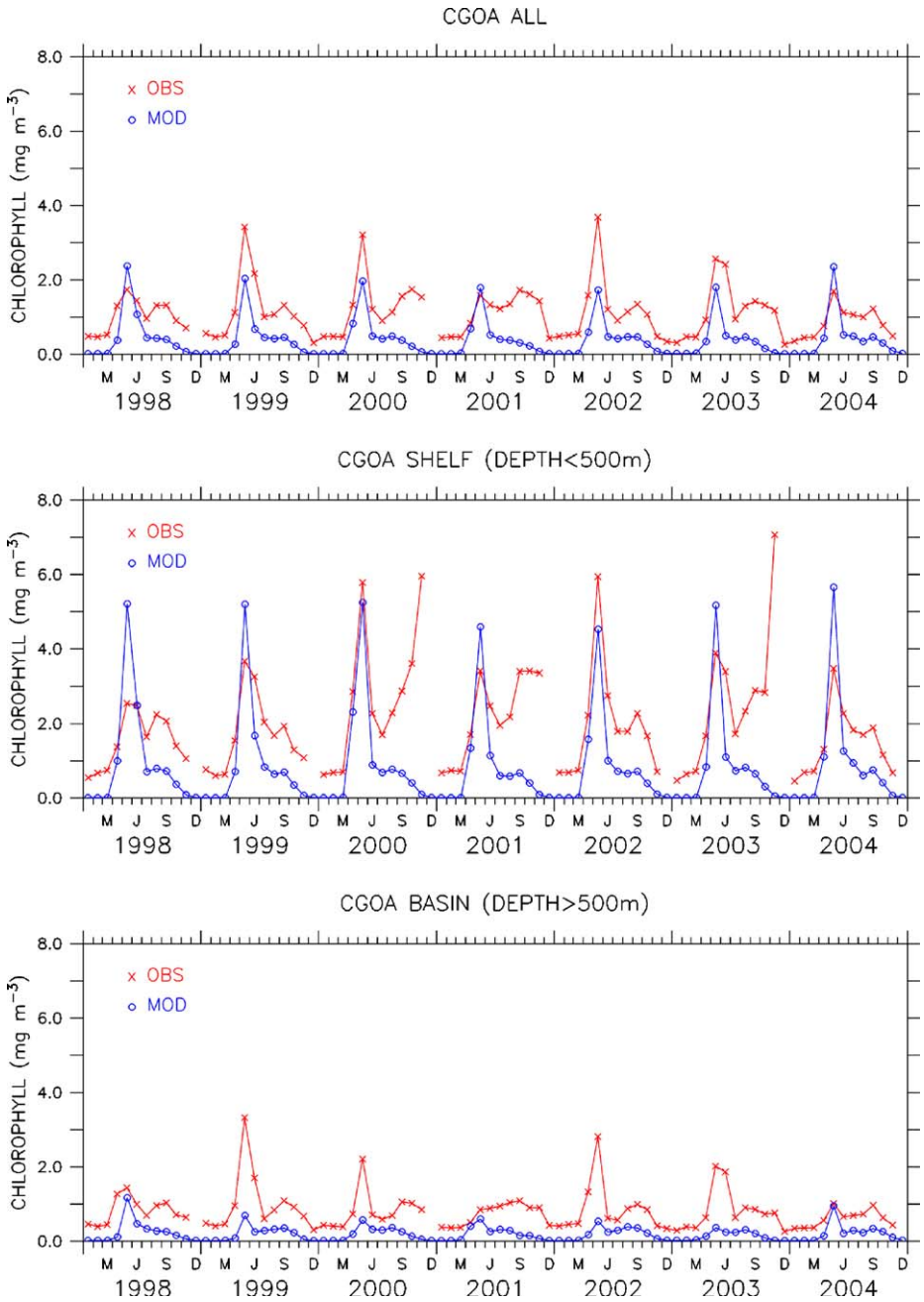

Fig. 5. Seven-year time series (1998–2004) for observed (SeaWiFS; x) and simulated (circles) surface chlorophyll concentrations (mg m^{-3}) spatially averaged over the entire CGOA domain (upper), over the CGOA shelf (middle), and over the CGOA basin (lower). The transition between the shelf and basin regions is arbitrarily defined as the 500-m isobath (approximate shelf break location). Source for SeaWiFS data: NOAA CoastWatch Program (http://coastwatch.pfel.noaa.gov).

CGOAs exhibits two distinct phytoplankton growth regimes (i.e. nitrate-limited and iron-limited), it is also instructive to differentiate between the shelf and the basin when evaluating the efficacy of the model. The transition between the shelf and the basin is arbitrarily chosen as the 500 m isobath, as it approximately coincides with the shelfbreak location. For the entire CGOA domain, the model predicts the timing of the spring bloom correctly, but underestimates the interannual variability in its magnitude. Simulated chlorophyll concentrations are on average lower than observed values by a factor of two in summer, and generally lack a noticeable peak during the fall bloom (Fig. 5, upper). On the shelf, the model adequately reproduces both the

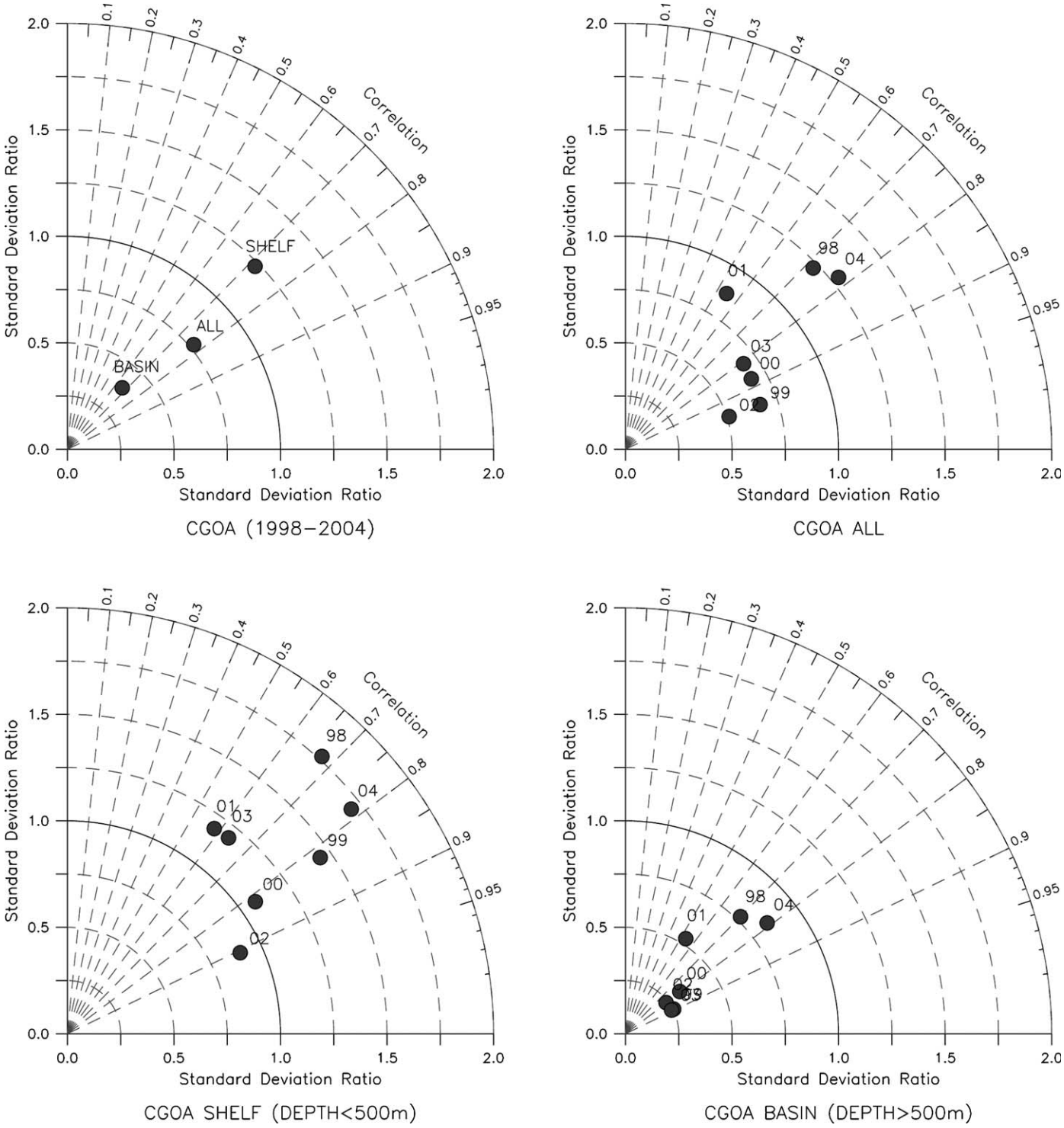

Fig. 6. Taylor diagrams for spatially averaged, monthly mean chlorophyll concentrations. Radial distance represents the ratio of simulated to observed (SeaWiFS) standard deviations and azimuthal angle represents model-data correlation. Observations coincide with location defined by standard deviation ratio and correlation equal to one. Upper left: diagram for 1998–2004 period separated by region (entire CGOA domain, CGOA shelf, and CGOA basin). Upper right: diagram for individual years over entire CGOA domain. Lower left: diagram for individual years over CGOA shelf. Lower right: diagram for individual years over CGOA basin. The transition between the shelf and basin regions is arbitrarily defined as the 500-m isobath (approximate shelf break location). Source for SeaWiFS data: NOAA CoastWatch Program (http://coastwatch.pfel.noaa.gov).

timing and magnitude of the spring bloom (Fig. 5, middle). Simulated peak chlorophyll concentrations are typically within 20–30% of the observed values, expect for 1998 and 2004 where they overestimate the magnitude of the spring bloom by ca. 50%. Summer and fall chlorophyll concentrations are, again, underestimated by the model, especially for the years with a strong fall bloom (e.g., 2001). Off the shelf, simulated and observed chlorophyll values both indicate a reduction in average phytoplankton concentrations compared to the shelf, but the model generally lacks the interannual variability present in the observations during spring (Fig. 5, lower).

To quantify the ability of the model to reproduce seasonal and interannual variability in monthly mean chlorophyll concentrations in the CGOA, model-data correlations and standard deviation ratios are presented in the form of Taylor diagrams (Taylor, 2001). Based on the entire 7-year period, model-data correlations are around 0.7 for chlorophyll concentrations spatially averaged over the entire domain, over the shelf only, and over the basin only (Fig. 6, upper left). In addition, simulated and observed chlorophyll concentrations have similar temporal variability (i.e. standard deviations) on the shelf, but the model underestimates temporal variability offshore by a factor of about three. When considering the entire domain, but evaluating each year individually, model-data comparisons indicate that the efficacy of the model varies significantly over the 7-year period (Fig. 6, upper right). For instance, correlations are as high as 0.8–0.95 for 1999, 2000, 2002, and 2003, but as low as 0.5 for 2001. In contrast, the temporal variability is more closely reproduced by the model in 2001, but underestimated by 25–50% for most years. 1998 and 2004 are the only years for which the model overestimates temporal variability. Focusing on the shelf region only, correlations are in the range of 0.6–0.9, with 2001 having the lowest value and 2002 the highest (Fig. 6, lower left). For most years, the model is able to reproduce the temporal variability present in the observations, with standard deviation ratios in the range 0.75–1.25 (except for 1998 and 2004 for which the ratio exceeds 1.5). For the basin, correlations are still in the range 0.5 (2001)–0.9 (2003), but the model underestimates the temporal variability by 50% or more, except for 1998 and 2004 (Fig. 6, lower right).

4.2. Seasonal variability (2001)

To further characterize the ability of the model to reproduce surface and sub-surface nitrate and chlorophyll concentrations, simulated variables are compared with in situ observations for 2001 along the Seward line (i.e. cross-shelf transect off Seward routinely sampled by the U.S. GLOBEC program; see Fig. 1, left panel). This specific year and location were selected because of the availability of concurrent in situ nitrate and chlorophyll (<5, 5–20, and $>20\,\mu m$ size-classes) measurements at three cross-shelf locations (inner-, mid-, and outer-shelf) for April, May, and July. Since the model contains only one phytoplankton size-class, it is instructive to compare simulated chlorophyll concentrations against observed chlorophyll concentrations from diatom (i.e. $>20\,\mu m$) and non-diatom (i.e. $<20\,\mu m$) contributions (Strom et al., 2006). Considering that model-data correlations are poorest in 2001, the results should also provide insight on the spatial and temporal discrepancies between simulated and observed concentrations.

For surface nutrients (Fig. 7, upper panels), the model reproduces the range of observed values on the inner- and mid-shelf, with a sharp decrease in nitrate concentrations during the

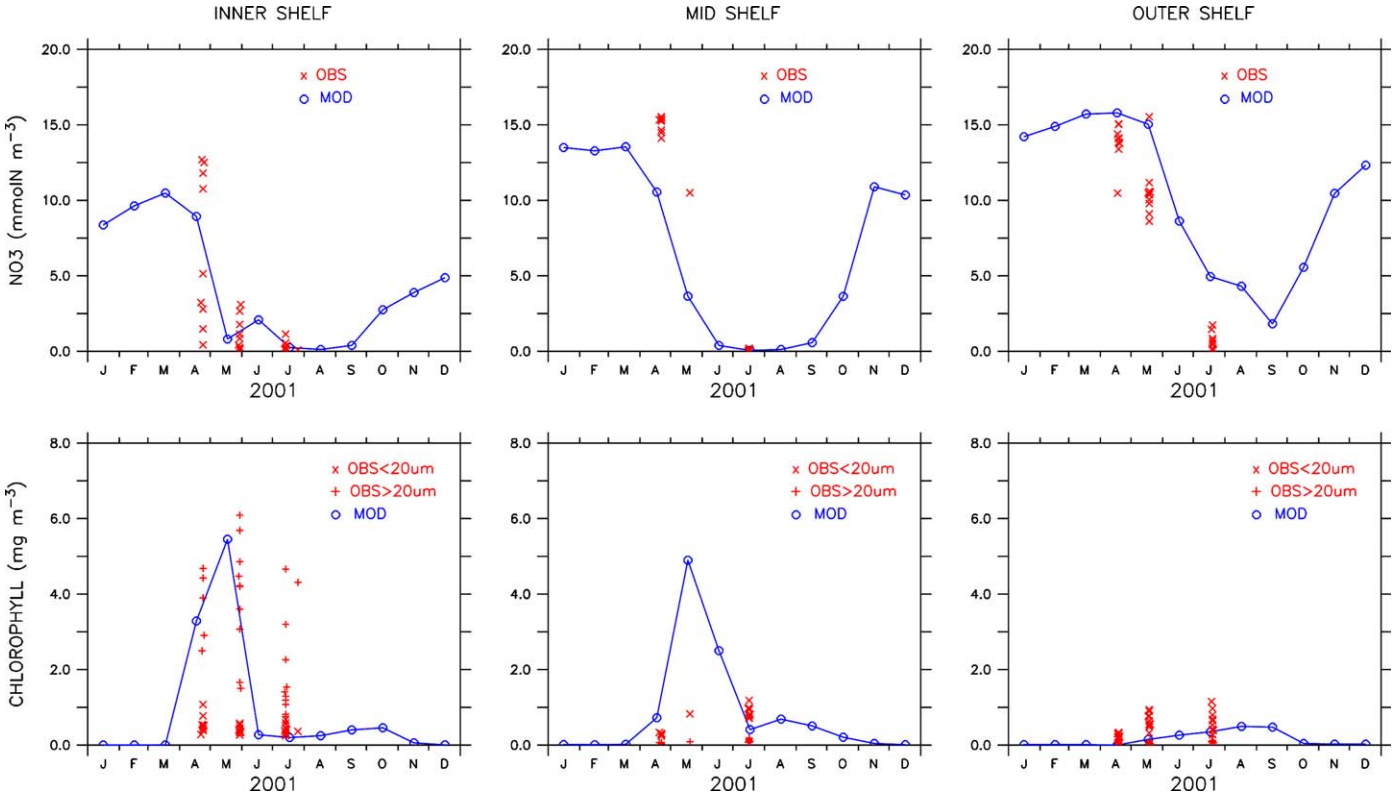

Fig. 7. Simulated and observed surface nitrate (mmolN m^{-3}; upper) and chlorophyll (mg m^{-3}; lower) concentrations along GLOEBC Seward line for 2001 (left: inner-shelf; center: mid-shelf; right: outer-shelf). In situ chlorophyll concentrations are separated into diatom ($>20\,\mu m$; +) and non-diatom ($<20\,\mu m$; $\times$) contributions. Symbols for in situ observations indicate individual daily measurements. Simulated concentrations (circles) are based on 2001 monthly means.

spring bloom and a complete drawdown during summer. On the outer-shelf, the model does not generate a sufficient nutrient drawdown in summer, resulting in simulated nitrate concentrations roughly five times larger than observed values (i.e. ca. 5 mmolN m^{-3} vs. 1 mmolN m^{-3}). For surface chlorophyll (Fig. 7, lower panels), the model reproduces the timing and magnitude of the diatom spring bloom on the inner-shelf, but underestimates summer chlorophyll concentrations at that location by a factor of roughly three. Since the monthly averaged nitrate drawdown is correctly predicted, the large diatom concentrations presumably result from episodic nutrient inputs on the inner shelf associated with tidal mixing or ACC frontal variability, neither process being accurately reproduced by the model due to the lack of tidal forcing and insufficient horizontal grid resolution. At the mid-shelf station, simulated and observed chlorophyll concentrations are comparable in April and July, but the model overestimates the magnitude of the spring bloom at that location. However, in situ observations for May at the mid-shelf station consist of only one measurement, rendering a proper model-data comparison difficult. On the outer-shelf, chlorophyll concentrations remain low throughout the year (i.e. no spring bloom), and the model underestimates the observations by about 50%, which is consistent with the weaker simulated nitrate drawdown.

Separating observed chlorophyll concentrations into diatom and non-diatom contributions clearly suggests that the CGOA cross-shelf phytoplankton community structure is not uniform, with diatoms dominating the inner-shelf, and smaller phytoplankton species dominating the mid- and outer-shelf. Since the ecosystem model contains only one phytoplankton size-class (parameterized to reproduce the timing and magnitude of the spring bloom), it is expected that simulated chlorophyll concentrations will not be as accurate in regions where the phytoplankton community is dominated by non-diatom species. In particular, since smaller oceanic phytoplankton species are less susceptible to iron limitation (Sunda and Huntsman, 1995), the lower chlorophyll concentration and lack of variability may be associated with an inadequate parameterization of the half-saturation Fe:C ratio in the ecosystem model.

For completeness, the ability of the model to reproduce the subsurface structure of observed chlorophyll profiles is also assessed. Since in situ chlorophyll measurements at the inner-, mid-, and outer-shelf stations along the Seward line typically cover three to four consecutive days (Strom et al., 2006), means and standard deviations are computed to facilitate comparison with the monthly averaged model fields. To provide a fair comparison, simulated chlorophyll concentrations are linearly interpolated from the monthly means to coincide with the centered day at which the in situ measurements were collected. To put the simulated chlorophyll profiles for 2001 into perspective, simulated "climatological" vertical profiles (i.e. based on the monthly means for 1998–2004) are also presented. On the inner-shelf (Fig. 8, left), the model reproduces correctly the vertical chlorophyll profiles corresponding to diatom contribution during the spring bloom (i.e. April and May). In summer, simulated chlorophyll concentrations are representative of the non-diatom

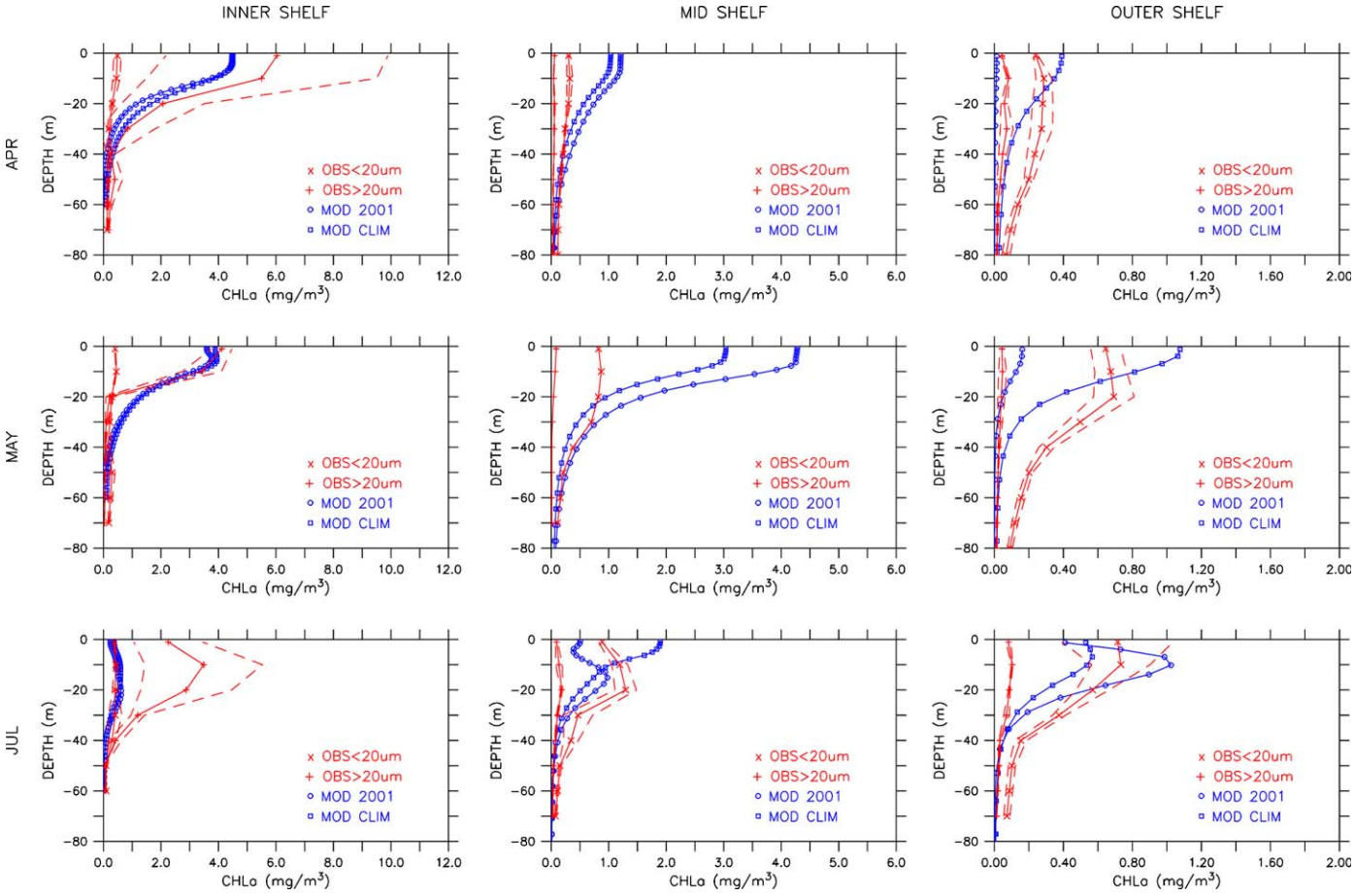

Fig. 8. Simulated and observed vertical chlorophyll (mg m^{-3}) concentration profiles along GLOEBC Seward line for April (upper), May (middle), and July (lower) 2001 (left: inner-shelf; center: mid-shelf; right: outer-shelf). In situ concentrations are separated into diatom (>20 μm; +) and non-diatom (<20 μm; ×) contributions. Solid lines represent mean of all in situ observations for the given month, and dashed lines indicate mean value ± one standard deviation. Simulated concentrations are based on 2001 (circles) and "climatological" (squares) monthly means. Note the different chlorophyll scales for the three shelf regions.

contribution, and significantly underestimate the diatom contribution. Furthermore, the 2001 and "climatological" vertical profiles are essentially identical, suggesting little interannual variability in the spring bloom chlorophyll concentrations on the inner shelf. On the mid-shelf (Fig. 8, center), observed chlorophyll concentrations indicate that the phytoplankton community structure is dominated by non-diatom species in both spring and summer. While the model reproduces the vertical structure and magnitude (within a factor of 2) of observed chlorophyll concentration profiles in April and July, it overestimates by a factor of 5 the magnitude of the spring bloom in May. The 2001 and "climatological" vertical profiles are mainly identical for April and May, but differ significantly in July, with the 2001 chlorophyll concentrations providing a closer agreement with observed values (i.e. predicting the presence of a subsurface chlorophyll maximum). On the outer-shelf (Fig. 8, right), the observed phytoplankton community structure is again dominated by non-diatom contributions, and the model results indicate significant interannual variability, as 2001 and "climatological" chlorophyll concentrations differ for all three months. In general, "climatological" chlorophyll concentrations provide a reasonable estimate of the vertical structure and magnitude of the non-diatom contribution, while the 2001 chlorophyll concentrations coincide more closely with the diatom contribution, except in summer.

Overall, the ecosystem model reproduces the magnitude and vertical structure of observed nitrate and chlorophyll concentrations for different seasons and cross-shelf locations. The largest discrepancies occur on the inner-shelf during summer (presumably due to a lack of tidal forcing and horizontal grid resolution to resolve the frontal dynamics of the ACC) and on the mid-shelf in May (overestimation of the spring bloom magnitude). Considering that the ecosystem model includes only one phytoplankton size-class (parameterized for diatoms), model-data differences are expected to increase when the phytoplankton community structure becomes dominated by non-diatom species (i.e. on the mid- and outer-shelf).

4.3. Sensitivity to forcing and model parameters

To assess the robustness of the ecosystem model results, a brief sensitivity study to forcing and model parameters is presented. Sensitivity to forcing compares simulated chlorophyll concentrations obtained with monthly mean, weekly mean, and daily mean surface forcing (e.g., wind stress, short-wave radiation). It also includes a case with monthly mean surface forcing, but with the presence of increased dissolved iron concentrations at depth in the basin (i.e. linear increase from 0.05 μmolFe m^{-3} at the surface to 0.6 μmolFe m^{-3} at 100 m depth; Hinckley et al., 2009). Sensitivity to model parameters compares simulated chlorophyll concentrations (monthly mean surface forcing) obtained with the default parameters, decreased zooplankton grazing, decreased detritus remineralization, and decreased Fe:C half-saturation constant.

Along the Seward line, monthly mean surface nitrate and chlorophyll concentrations exhibit little sensitivity to the temporal resolution of surface forcing on the inner- and mid-shelf (Fig. 9). Using weekly or daily mean forcing instead of monthly mean forcing, leads to a slight increase of the fall bloom magnitude on the inner-shelf, and a slight decrease of the spring bloom magnitude on the mid-shelf. On the outer-shelf, increasing the

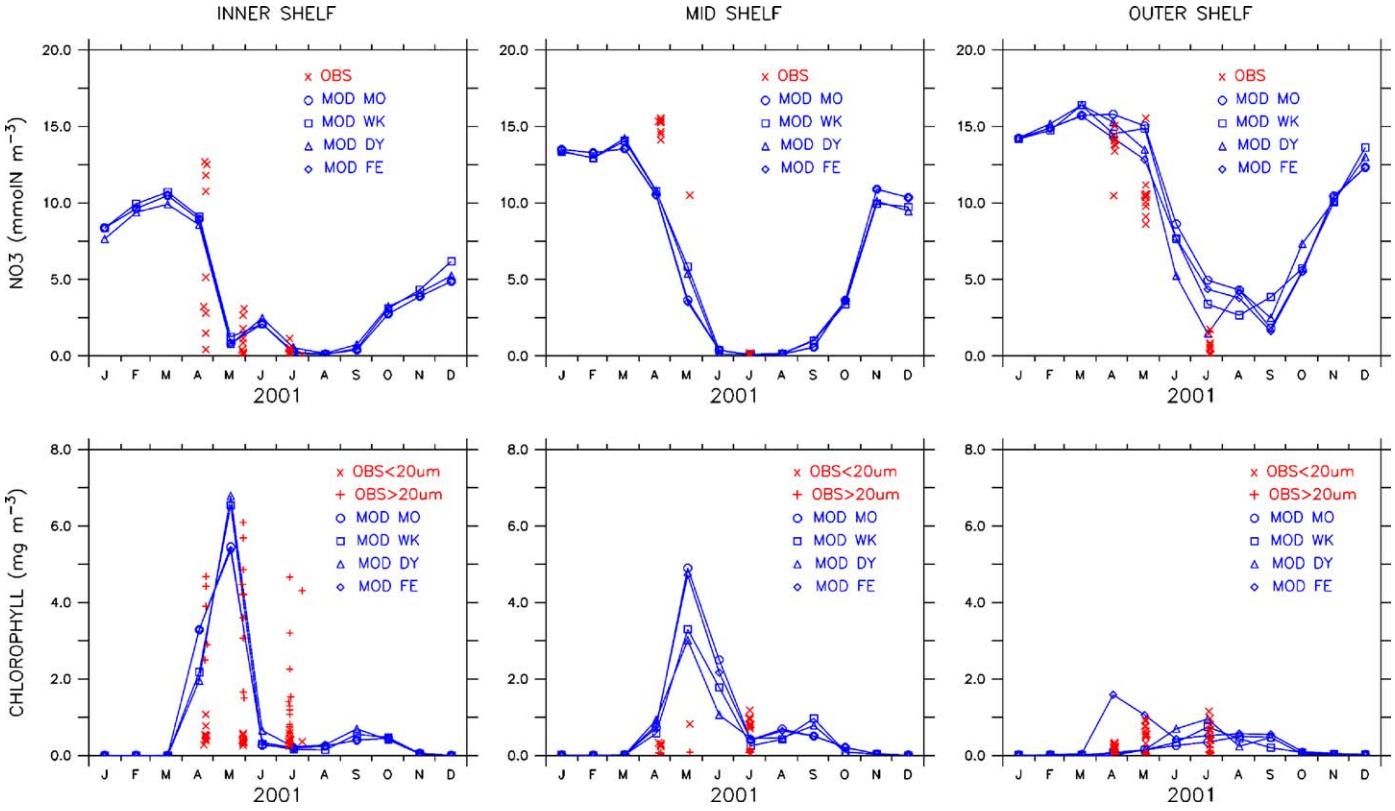

Fig. 9. Simulated and observed surface nitrate (mmolN m^{-3}; upper) and chlorophyll (mg m^{-3}; lower) concentrations along GLOEBC Seward line for 2001 (left: inner-shelf; center: mid-shelf; right: outer-shelf). In situ chlorophyll concentrations are separated into diatom (>20 μm; +) and non-diatom (<20 μm; ×) contributions. Symbols for in situ observations indicate individual daily measurements. Simulated concentrations represent cases with monthly mean (MO; circles), weekly mean (WK; squares), and daily mean (DY; triangles) surface forcing, as well as with increased dissolved iron concentration at depth in basin (FE; diamonds).

temporal resolution of the surface forcing from monthly to daily mostly results in larger (by a factor of roughly 3) nitrate drawdown and chlorophyll concentrations in summer. As expected, increasing dissolved iron concentrations at depth in the basin does not impact nitrate and chlorophyll concentrations on the inner- and mid-shelf. However, on the outer-shelf, the presence of higher subsurface dissolved iron concentrations leads to an increase in spring and summer chlorophyll concentrations.

The impact of surface forcing and increased subsurface dissolved iron concentrations on the vertical structure of chlorophyll concentrations is also modest, with the main differences being (as already discussed above): a decrease in the magnitude of the spring bloom on the mid-shelf with increasing temporal resolution in surface forcing, and an increase in chlorophyll concentrations on the outer-shelf with increasing dissolved iron concentration at depth (Fig. 10).

While limited to only three parameters (zooplankton grazing rate, detritus remineralization rate, and phytoplankton Fe:C half-saturation constant), the sensitivity study is focused on describing the potential effects of grazing pressure, recycled production, and iron limitation threshold on phytoplankton growth and abundance in the CGOA. For surface fields (Fig. 11), decreasing the zooplankton grazing rate by 50% does not significantly modify nitrate and chlorophyll concentration on the mid- and outer-shelf, but leads to an increase in the spring bloom magnitude in May (by ca. 30%) and a slower phytoplankton decay into summer (i.e. larger chlorophyll concentrations in June and July). Reducing the grazing pressure also results in a complete nitrate drawdown in summer on the inner-shelf, where the default parameters yield residual surface nitrate values in the range of 2–3 mmolN m^{-3}. Decreasing the detritus remineralization rate by an order of magnitude (i.e. from 1.0 to 0.1 day^{-1}) does not lead to significant changes in nitrate and chlorophyll concentrations on the mid- and outer-shelf, but reduces overall chlorophyll concentrations on the inner-shelf. Decreasing detritus remineralization also results in inner-shelf nitrate concentrations near zero in summer, thereby suggesting that summer chlorophyll concentrations with the default parameters are mainly associated with recycled production. Since the ecosystem model does not differentiate between nitrate- and ammonium-driven phytoplankton growth (i.e. only one nitrogen compartment), it is difficult to quantify exactly the respective contributions of new and recycled production on the CGOA shelf. Decreasing the phytoplankton Fe:C half-saturation constant by 50% does not modify nitrate and chlorophyll concentrations on the inner- and mid-shelf (which is expected since phytoplankton growth at these two locations is primarily nitrate-limited), but results in higher chlorophyll concentrations on the outer-shelf, particularly during the spring bloom. Reducing the iron limitation threshold also increases nitrate utilization in summer on the outer-shelf, but residual nitrate concentrations in July are still higher than observed values by a factor of roughly 4.

For subsurface fields (Fig. 12), the results are generally independent of ecosystem model parameterization, except in

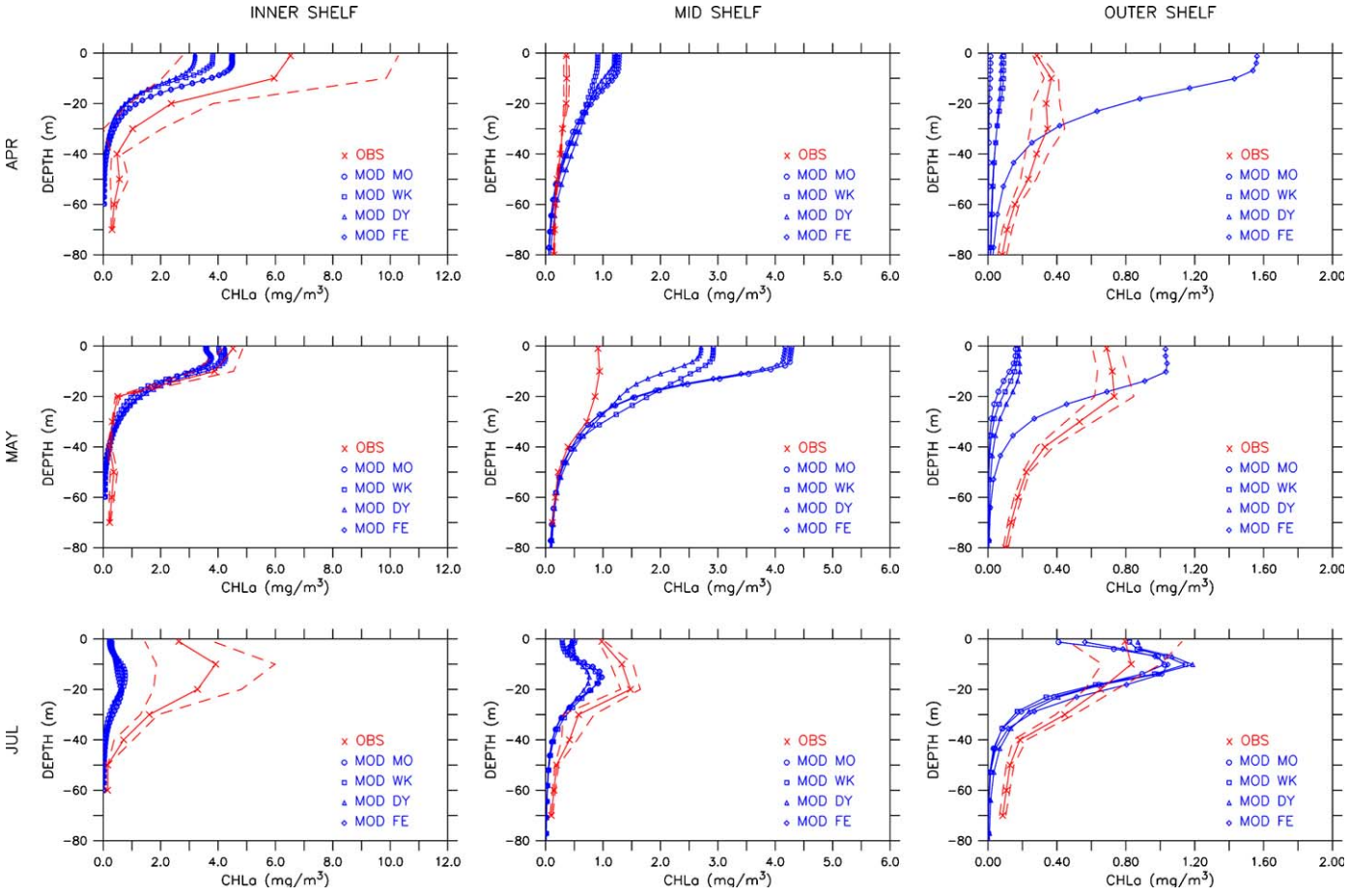

Fig. 10. Simulated and observed vertical chlorophyll (mg m^{-3}) concentration profiles along GLOEBC Seward line for April (upper), May (middle), and July (lower) 2001 (left: inner-shelf; center: mid-shelf; right: outer-shelf). In situ concentrations (×) indicate total chlorophyll (diatom plus non-diatom contributions). Solid lines represent mean of all in situ observations for the given month, and dashed lines indicate mean value ± one standard deviation. Simulated concentrations represent cases with monthly mean (MO; circles), weekly mean (WK; squares), and daily mean (DY; triangles) surface forcing, as well as with increased dissolved iron concentration at depth in basin (FE; diamonds). Note the different chlorophyll scales for the three shelf regions.

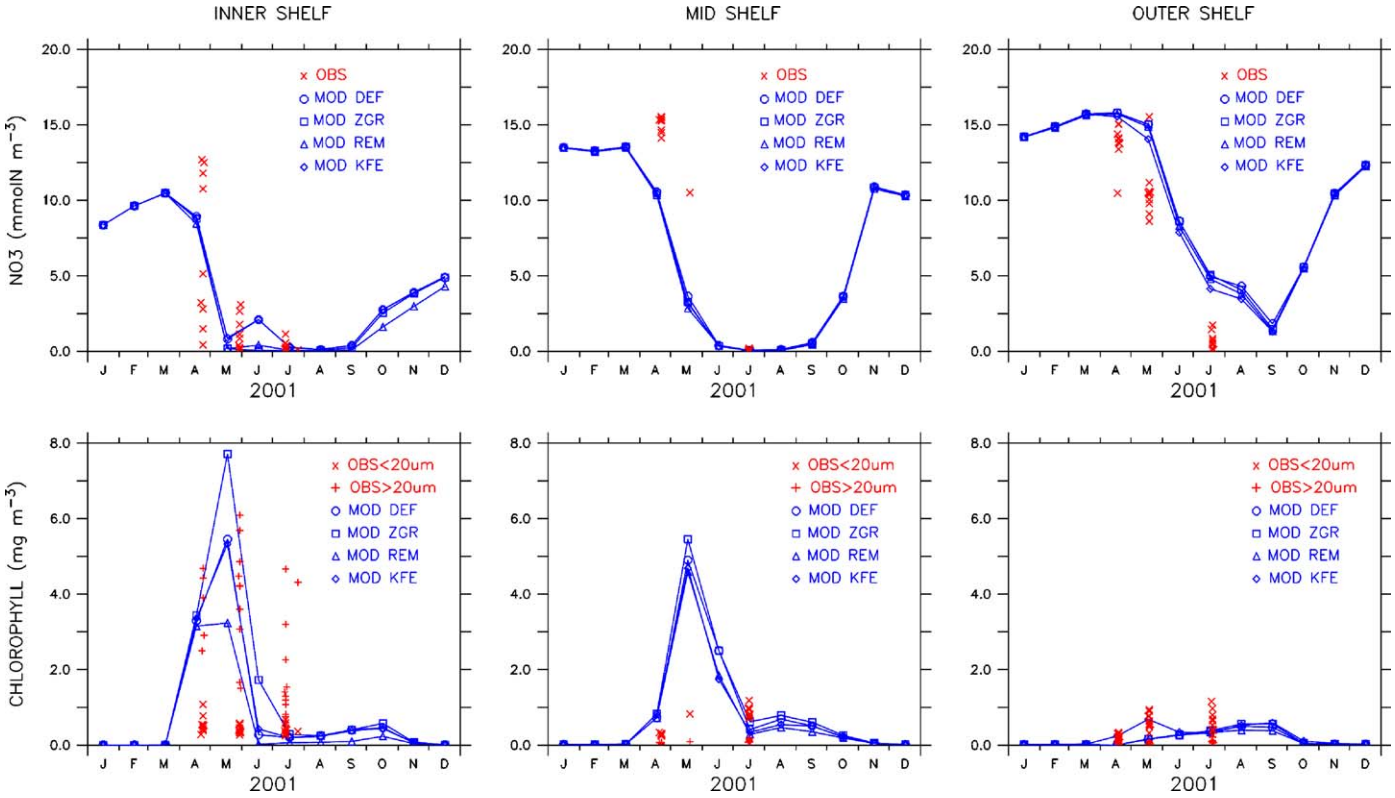

Fig. 11. Simulated and observed surface nitrate (mmolN m^{-3}; upper) and chlorophyll (mg m^{-3}; lower) concentrations along GLOEBC Seward line for 2001 (left: inner-shelf; center: mid-shelf; right: outer-shelf). In situ chlorophyll concentrations are separated into diatom ($>2\,\mu$m; +) and non-diatom ($<20\,\mu$m; $\times$) contributions. Symbols for in situ observations indicate individual daily measurements. Simulated concentrations represent cases with default parameters (DEF; circles), 50% decrease in zooplankton grazing (ZGR; squares), order of magnitude decrease in detritus remineralization (REM; triangles), and 50% decrease in phytoplankton Fe:C half-saturation constant (KFE; diamonds).

summer on the inner-shelf and in spring on the outer-shelf. On the inner-shelf, decreasing zooplankton grazing by half significantly enhances subsurface summer chlorophyll concentrations (from less than 1 to ca. 3 mmolN m^{-3} at 20-m depth), and results in a vertical profile more closely approximating in situ observations. On the outer-shelf, decreasing the phytoplankton Fe:C half-saturation constant by half significantly increases chlorophyll concentrations in the upper water column (i.e. above 20-m depth) during spring, leading to a better agreement between modeled and observed vertical profiles. Since the outer-shelf phytoplankton community structure is dominated by non-diatom species, the results are consistent with the fact that smaller oceanic species are less susceptible to iron limitation than larger coastal species.

Finally, the sensitivity study is extended to the full CGOA domain for 2001 with Taylor diagrams comparing model results and SeaWiFS observations in terms of spatially averaged chlorophyll concentrations over the entire region, over the shelf only, and over the basin only (Fig. 13). Overall, the results confirm the influence of forcing and parameter selection described for the Seward line. For instance, while the temporal resolution of surface forcing does not significantly change standard deviations and correlations based on monthly mean values, the presence of increased dissolved iron concentrations at depth enhances variability on the outer-shelf, but also reduces model-data correlation by half. For model parameters, decreasing zooplankton grazing pressure increases model variability and improves model-data correlations (by ca. 10%) for both on and off the shelf. Decreasing the phytoplankton iron limitation threshold increases variability at the shelfbreak and in the basin, but has no impact on the shelf. Decreasing the detritus remineralization rate does not lead to significant changes either on the shelf or in the basin.

5. Discussion

Because of the distinct phytoplankton growth regimes on the shelf (i.e. nitrate-limited) and offshore (i.e. iron-limited) in the northwestern CGOA, a successful lower trophic level ecosystem model must at least include these two nutrients to reproduce the dominant spatial and temporal chlorophyll patterns in the region. Furthermore, since atmospheric wind regime in the northwestern CGOA is predominantly downwelling-favorable, coupling the ecosystem model to a regional ocean circulation model is necessary to include the physical processes that seasonally replenish nutrients into the euphotic zone (e.g., vertical mixing, cross-shelf transport).

For the purpose of studying long-term (i.e. interannual to decadal) ecosystem response to oceanic and atmospheric forcing, computational grids must be kept to manageable sizes, leading to a trade-off in the accuracy with which certain physical and biological processes are represented. For instance, while the coupled ocean circulation-ecosystem model described here adequately reproduces the spring bloom dynamics on the inner-shelf, the low summer chlorophyll concentrations are presumably attributable in part to the coarse horizontal resolution and lack of tidal forcing, as summer primary production on the CGOA shelf may be driven significantly by tidal mixing and bathymetric steering of the circulation (Ladd et al., 2005). It is expected that

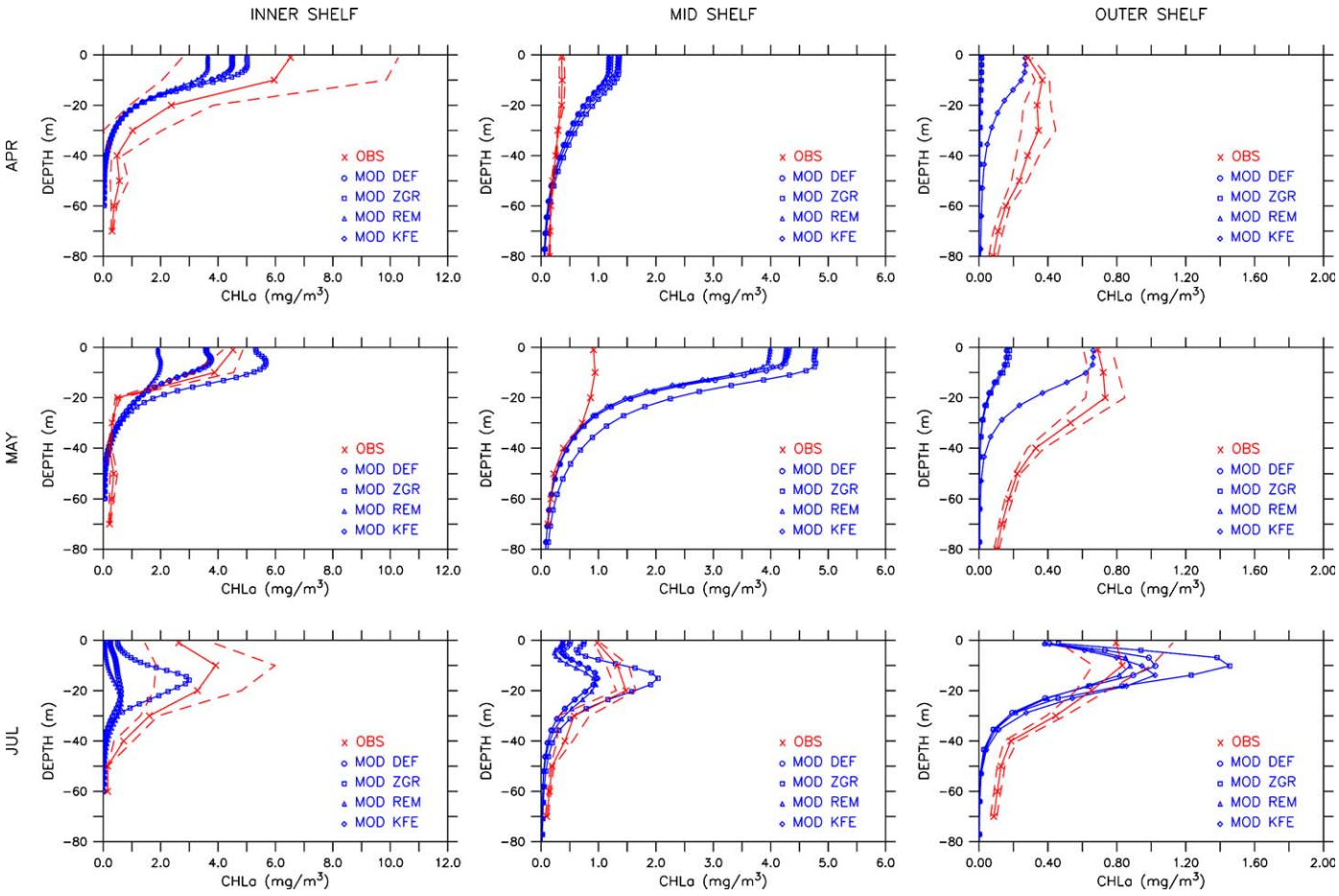

Fig. 12. Simulated and observed vertical chlorophyll (mg m^{-3}) concentration profiles along GLOEBC Seward line for April (upper), May (middle), and July (lower) 2001 (left: inner-shelf; center: mid-shelf; right: outer-shelf). In situ concentrations (×) indicate total chlorophyll (diatom plus non-diatom contributions). Solid lines represent mean of all in situ observations for the given month, and dashed lines indicate mean value ± one standard deviation. Simulated concentrations represent cases with default parameters (DEF; circles), 50% decrease in zooplankton grazing (ZGR; squares), order of magnitude decrease in detritus remineralization (REM; triangles), and 50% decrease in phytoplankton Fe:C half-saturation constant (KFE; diamonds). Note the different chlorophyll scales for the three shelf regions.

increasing the horizontal resolution in the model would help resolve some of the discrepancies between simulated and observed chlorophyll concentrations, especially on the inner shelf and in regions of strong topographic gradients. Similarly, while the model reproduces the transition from a nitrate-limited to an iron-limited phytoplankton growth regime with offshore distance, simulated chlorophyll concentrations off the shelf generally lack the temporal variability present in remotely sensed observations. Since the spatial and temporal variability along the CGOA shelfbreak is strongly influenced by oceanic mesoscale activity (Okkonen et al., 2003; Brickley and Thomas, 2004; Ladd, 2007), the accuracy with which the model captures the timing and intensity of cross-shelf and vertical transport events associated with eddy passages will significantly impact its ability to predict seasonal and interannual ecosystem variability off the shelf. Furthermore, since iron limitation is a critical biological process in the CGOA, additional in situ measurements of iron concentrations would improve lower trophic level ecosystem models for the region by more accurately defining cross-shelf phytoplankton growth regimes.

The level of complexity and parameterization of the ecosystem model will also contribute significantly to the accuracy with which simulations reproduce the spatial and temporal variability in chlorophyll concentrations. For instance, since the CGOA phytoplankton community structure changes from diatom-dominated on the shelf to non-diatom-dominated at the shelfbreak and in the basin (Strom et al., 2006), the addition of a second phytoplankton size-class to the ecosystem model would lead to a more accurate response to environmental cross-shelf gradients. With only one size class parameterized for diatoms, the present model still captures the dominant patterns of nitrate and iron limitation on phytoplankton growth, but parameter sensitivity indicates that reducing the phytoplankton Fe:C half-saturation constant (i.e. smaller oceanic species have lower cellular iron requirements (Sunda and Huntsman, 1995)) increases the temporal variability off the shelf and provides a more consistent approximation of that associated with observations.

Parameter sensitivity studies also suggest that zooplankton grazing exerts a significant control on phytoplankton concentrations, in addition to growth limitation by light, nitrate, and iron. Reducing zooplankton grazing pressure increases subsurface summer phytoplankton concentrations on the inner- and mid-shelf by nearly an order of magnitude, leading to a closer agreement with in situ vertical chlorophyll profiles. Furthermore, reducing zooplankton grazing rates also improves spatially averaged model-data correlation over the entire CGOA domain, as well as increases the temporal variability in simulated chlorophyll concentrations. In fact, the lack of a significant fall bloom in the model could possibly be related to excessive zooplankton grazing pressure, especially since copepods (i.e. the dominant zooplankton species on the shelf) migrate offshore and deeper in late summer (Coyle and Pinchuk, 2005). Therefore,

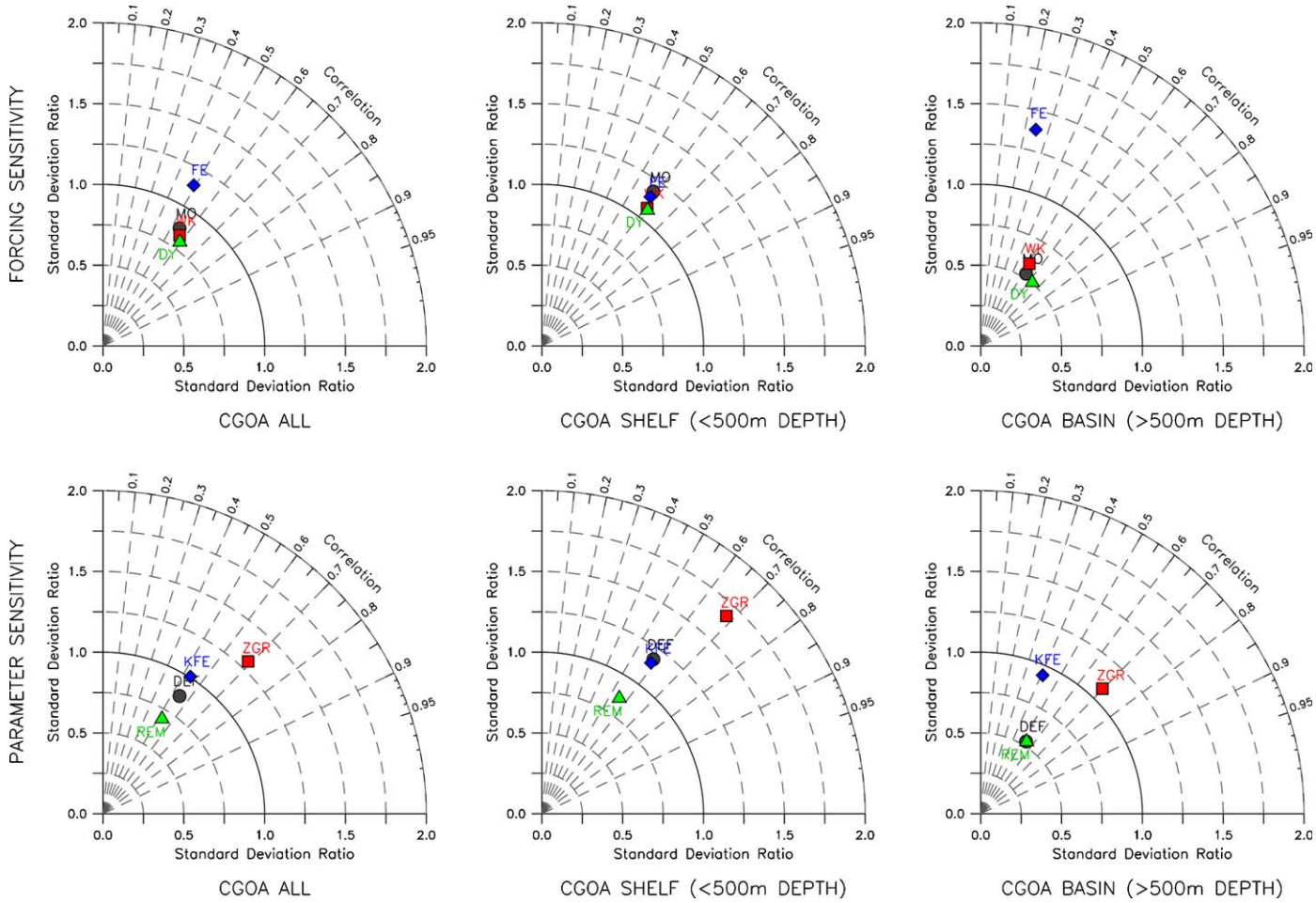

Fig. 13. Taylor diagrams for spatially averaged, monthly mean chlorophyll concentrations for 2001 over entire CGOA domain (left); CGOA shelf (center), and CGOA basin (right). Radial distance represents the ratio of simulated to observed (SeaWiFS) standard deviations and azimuthal angle represents model-data correlation. Observations coincide with location defined by standard deviation ratio and correlation equal to one. Upper: diagrams for simulations with monthly mean (MO; circles), weekly mean (WK; squares), and daily mean (DY; triangles) surface forcing, as well as with increased dissolved iron concentration at depth in basin (FE; diamonds). Lower: diagrams for simulations with default parameters (DEF; circles), 50% decrease in zooplankton grazing (ZGR; squares), order of magnitude decrease in detritus remineralization (REM; triangles), and 50% decrease in phytoplankton Fe:C half-saturation constant (KFE; diamonds). The transition between shelf and basin regions is arbitrarily defined as the 500-m isobath (approximate shelf break location). Source for SeaWiFS data: NOAA CoastWatch Program (http://coastwatch.pfel.noaa.gov).

including a seasonal relaxation of zooplankton grazing rates in summer and fall might represent an important improvement to the ecosystem model, and could help reproduce more accurately the phytoplankton dynamics associated with the fall bloom.

6. Conclusion

Despite obvious discrepancies associated with physical processes not adequately represented in the ocean circulation model (e.g., ACC frontal dynamics), parameter uncertainties in the ecosystem model (e.g., zooplankton grazing rates), and lack of data on dissolved iron cross-shelf gradients, simulated nitrate and chlorophyll concentrations exhibit significant similarities with available remotely sensed (SeaWiFS) and in situ (GLOBEC) observations on seasonal and interannual timescales. Model-data correlations based on spatially averaged, monthly mean chlorophyll concentrations range between 0.5 (2001) and 0.9 (1999, 2002) for individual years, with an average of about 0.7 over the whole 1998–2004 period. Simulated and observed temporal variability are comparable on the shelf (i.e., inshore of the 500 m isobath), but the model underestimates on average by a factor of 2 the seasonal and interannual variability present in the observations at the shelfbreak and in the basin. Since the model generally underestimates the magnitude of the fall bloom, simulated chlorophyll concentrations provide a closer fit to the observations for years with a strong spring bloom and weak fall bloom. For instance, the lowest model-data correlation in 2001 coincides with a year during which the spring and fall blooms had comparable magnitudes (i.e. weak spring bloom and strong fall bloom). Despite a weaker correlation with remotely sensed observations, the model still provides a reasonably accurate description of the vertical and cross-shelf nitrate and chlorophyll concentrations on a seasonal timescale when compared to in situ observations for 2001.

While the ecosystem model represents a simple approximation of the complex lower trophic level dynamics of the northwestern CGOA (i.e., only two limiting nutrient (nitrate and iron) and one size class for phytoplankton and zooplankton), simulated chlorophyll concentrations reproduce the main characteristics of the spring bloom, high shelf primary production, and HNLC environment offshore. The model also provides insight on the importance of micro- and macro-nutrient limitation on the shelf and offshore, with the shelfbreak region acting as a transition zone where the availability of both nitrate and iron impacts phytoplankton growth. The ability of the model to differentiate between

nitrate- and iron-limited growth conditions, as well as to identify their spatial and temporal occurrences, is a first step towards understanding the role of environmental gradients in shaping the complex CGOA phytoplankton community structure. Sensitivity studies with different model configurations are also critical to investigate which physical and biological processes predominantly control the overall variability in nutrient and chlorophyll concentrations. For instance, while monthly mean chlorophyll concentrations exhibit little sensitivity to daily vs. monthly averaged surface forcing, changes in zooplankton grazing rates have a significant impact on seasonal variations in cross-shelf and vertical phytoplankton concentrations. In conclusion, the model provides a useful platform to refine simulations of the seasonal and interannual CGOA lower trophic level ecosystem dynamics, as well as to build greater complexity into future ecosystem models for the region.

Acknowledgements

The research described here was supported by a grant from the National Science Foundation Biological Oceanography Program (OCE 0624776). Any opinions, findings and conclusions or recommendations expressed here are those of the authors and do not necessarily reflect the views of the National Science Foundation. S. Strom, T. Weingartner, and T. Whitledge are acknowledged for making available in situ chlorophyll and nitrate observations collected along the Seward line during the GLOBEC program. SeaWiFS chlorophyll data are courtesy of the NOAA CoastWatch Program, NASA's Goddard Space Flight Center, and GeoEye. Also thanked are A. Hermann for facilitating access to dissolved iron data and GLOBEC observations, and H. Arango for tireless coding and debugging of ROMS. Comments received from H. Batchelder and two anonymous reviewers were greatly appreciated. This research in U.S. GLOBEC contribution number 623.

References

Archer, D.E., Johnson, K., 2000. A model of the iron cycle in the ocean. Global Biogeochemical Cycles 14 (1), 269–279.

Aumont, O., Maier-Reimer, E., Blain, S., Monfray, P., 2003. An ecosystem model of the global ocean including Fe, Si, P colimitation. Global Biogeochemical Cycles 17 (2), 1060.

Brickley, P.J., Thomas, A.C., 2004. Satellite-measured seasonal and inter-annual chlorophyll variability in the Northeast Pacific and Coastal Gulf of Alaska. Deep-Sea Research II 51, 229–245.

Bruland, K.W., Rue, E.L., Smith, G.J., 2001. The influence of iron and macronutrients in coastal upwelling regimes off central California: implications for extensive blooms of large diatoms. Limnology and Oceanography 46, 1661–1674.

Bruland, K.W., Rue, E.L., Smith, G.J., DiTullio, G.R., 2005. Iron, macronutrients and diatom blooms in the Peru Upwelling regime: brown and blue waters of Peru. Marine Chemistry 93, 81–103.

Budgell, W.P., 2005. Numerical simulation of ice-ocean variability in the Barents Sea region: towards dynamical downscaling. Ocean Dynamics 55, 370–387.

Chai, F., Dugdale, R.C., Peng, T.-H., Wilkerson, F.P., Barber, R.T., 2002. One dimensional ecosystem model of the equatorial Pacific upwelling system. Part I: model development and silicon and nitrogen cycle. Deep-Sea Research II 49, 2713–2745.

Coyle, K.O., Pinchuk, A.I., 2005. Seasonal cross-shelf distribution of major zooplankton taxa on the northern Gulf of Alaska shelf relative to water mass properties, species depth preferences and vertical migration behavior. Deep-Sea Research II 52, 217–245.

Combes, V., Di Lorenzo, E., 2007. Intrinsic and forced interannual variability of the Gulf of Alaska mesoscale circulation. Progress in Oceanography, 75, 266–286, doi:10.1016/j.pocean.2007.08.011.

Conkright, M.E., Boyer, T.P., 2002. World Ocean Atlas 2001: Objective Analyses, Data Statistics, and Figures, CD-ROM Documentation. National Oceanographic Data Center, Silver Spring, MD, 17pp.

Curchitser, E.N., Haidvogel, D.B., Hermann, A.J., Dobbins, E.L., Powell, T.M., Kaplan, A., 2005. Multi-scale modeling on the North Pacific Ocean: assessment and analysis of simulated basin-scale variability (1996–2003). Journal of Geophysical Research 110 (C11021).

Denman, K.L., Peña, M.A., 1999. A coupled 1-D biological/physical model of the northeastern subarctic Pacific Ocean with iron limitation. Deep-Sea Research II 46, 2877–2908.

Denman, K.L., Voelker, C., Peña, M.A., Rivkin, R.B., 2006. Modelling the ecosystem response to iron fertilization in the subarctic NE Pacific: the influence of grazing, and Si and N cycling on CO_2 drawdown. Deep-Sea Research II 53, 2327–2352.

Franks, P.J., Wroblewski, J.S., Flierl, G.R., 1986. Behavior of a simple plankton model with food-level acclimation by herbivores. Marine Biology 91, 121–129.

Fujii, M., Yoshie, N., Yamanaka, Y., Chai, F., 2005. Simulated biogeochemical responses to iron enrichments in three high nutrient, low chlorophyll (HNLC) regions. Progress in Oceanography 64, 307–324.

Gregg, W.W., Schopf, P.S., Casey, N.W., 2003. Phytoplankton and iron: validation of a global three-dimensional ocean biogeochemical model. Deep-Sea Research II 50, 3134–3169.

Haidvogel, D.B., Arango, H.G., Hedstrom, K., Beckmann, A., Malanotte-Rizzoli, P., Shchepetkin, A.F., 2000. Model evaluation experiments in the North Atlantic Basin: simulations in nonlinear terrain-following coordinates. Dynamics Atmosphere Oceans 32, 239–281.

Hinckley, S., Coyle, K.O., Gibson, G., Hermann, A.J., Dobbins, E.L., 2009. A biophysical NPZ model with iron for the Gulf of Alaska: reproducing the differences between an oceanic HNLC ecosystem and a classical northern temperate shelf ecosystem. Deep-Sea Research II 56 (24), 2520–2536.

Hofmann, E.E., 1988. Plankton dynamics on the outer southeastern US continental shelf, III, A coupled physical-biological model. Journal Marine Research 46 (4), 919–946.

Jiang, M., Chai, F., 2004. Iron and silicate regulation of new and export production in the equatorial Pacific: A physical-biological model study. Geophysical Research Letters 31.

Kishi, M.J., Kashiwai, M., Ware, D.M., Megrey, B.A., Eslinger, D.L., Werner, F.E., Aita, M.N., Azumaya, T., Fujii, M., Hashimoto, S., Huang, D., Iizumi, H., Ishida, Y., Kang, S., Kantakov, G.A., Kim, H., Komatsu, K., Navrotsky, V.V., Lan Smith, S., Tadokoro, K., Tsuda, A., Yamamura, O., Yamanaka, Y., Yokouchi, K., Yoshie, N., Zhang, J., Zuenko, Y.I., Zvalinsky, V.I., 2007. NEMURO—a lower trophic level model for the North Pacific marine ecosystem. Ecological Modelling 202, 12.

Ladd, C., Stabeno, P., Cokelet, E.D., 2005. A note on cross-shelf exchange in the northern Gulf of Alaska. Deep-Sea Research II 52, 667–679.

Ladd, C., 2007. Interannual variability of the Gulf of Alaska eddy field. Geophysical Research Letters 34, L11605.

Lam, P.J., Bishop, J.K.B., Henning, C.C., Marcus, M.A., Waychunas, G.A., Fung, I.Y., 2006. Wintertime phytoplankton bloom in the subarctic Pacific supported by continental margin iron. Global Biogeochemical Cycles 20, GB1006.

Large, W.G., McWilliams, J.C., Doney, S.C., 1994. Oceanic vertical mixing: A review and a model with a nonlocal boundary layer parameterization. Reviews of Geophysics 29, 363–403.

Large, W.G., Yeager, S.G., 2004. Diurnal to decadal global forcing for ocean and Sea-Ice models: the data sets and flux climatologies. NCAR Technical Note 460.

Leonard, C.L., McClain, C.R., Murtugudde, R., Hofmann, E.E., Harding, L.W., 1999. An iron-based ecosystem model of the central equatorial Pacific. Journal of Geophysical Research 1004 (C1), 1325–1341.

Lima, I.D., Olson, D.B., Doney, S.C., 2002. Biological response to frontal dynamics and mesoscale variability in oligotrophic environments: biological production and community structure. Journal Geophysical Research 107 (C8), 3111.

Martin, J.H., Fitzwater, S.E., 1988. Iron deficiency limits phytoplankton growth in the north-east Pacific subarctic. Nature 331, 341–343.

Martin, J.H., Gordon, R.M., Fitzwater, S.E., Broenkow, W.W., 1989. VERTEX: phytoplankton/iron studies in the Gulf of Alaska. Deep-Sea Research 36 (5), 649–680.

Moore, J.K., Doney, S.C., Kleypas, J.A., Glover, D.M., Fung, I.Y., 2002. An intermediate complexity marine ecosystem model for the global domain. Deep-Sea Research II 49, 403–462.

Okkonen, S.R., Weingartner, T.J., Danielson, S.L., Musgrave, D.L., 2003. Satellite and hydrographic observations of eddy-induced shelf-slope exchange in the northwestern Gulf of Alaska. Journal of Geophysical Research 108 (C2), 3033.

Powell, T.M., Lewis, C.V.W., Curchitser, E.N., Haidvogel, D.B., Hermann, A.J., Dobbins, E.L., 2006. Results from a three-dimensional, nested, biological-physical model of the California Current System and comparisons with statistics from satellite imagery. Journal of Geophysical Research 111 (C0), 7018.

Reed, R.K., 1984. Flow of the Alaskan Stream and its variations. Deep-Sea Research 31 (4), 369–386.

Royer, T.C., 1981. Baroclinic transport in the Gulf of Alaska. Part II: fresh water driven Alaska Coastal Current. Journal of Marine Research 39, 251–266.

Royer, T.C., 1998. Coastal processes in the northern North Pacific. In: Robinson, A.R., Brink, K.H. (Eds.), The Sea. John Wiley & Sons, New York, NY, pp. 395–414.

Shaked, Y., Kutsha, A.B., Morel, F.M.M., 2005. A general kinetic model for iron acquisition by eukaryotic phytoplankton. Limnology and Oceanography 50 (3), 872–882.

Shchepetkin, A.F., McWilliams, J.C., 2005. The regional oceanic modeling system (ROMS): a split-explicit, free-surface, topography-following-coordinate oceanic model. Ocean Modelling 9, 347–404.

Spitz, Y.H., Newberger, P.A., Allen, J.S., 2003. Ecosystem response to upwelling off the Oregon coast: behavior of three nitrogen-based models. Journal of Geophysical Research 108 (C3), 3062.

Stabeno, P.J., Bond, N.A., Hermann, A.J., Kachel, N.B., Mordy, C.W., Overland, J.E., 2004. Meteorology and oceanography of the Northern Gulf of Alaska. Continental Shelf Research 24, 859–897.

Strom, S.L., Brady Olson, M., Macri, E.L., Mordy, C.W., 2006. Cross-shelf gradient in phytoplankton community structure, nutrient utilization, and growth rate in the coastal Gulf of Alaska. Marine Ecology Progress Series 328, 75–92.

Strom, S.L., Macri, E.L., Brady Olson, M., 2007. Microzooplankton grazing in the coastal Gulf of Alaska: Variations in top-down control of phytoplankton. Limnology and Oceanography 52 (4), 1480–1494.

Taylor, K.E., 2001. Summarizing multiple aspects of model performance in single diagram. Journal Geophysical Research 106 (D7), 7183–7192.

Sunda, W., Huntsman, S.A., 1995. Iron uptake and growth limitation in oceanic and coastal phytoplankton. Marine Chemistry 50, 189–206.

Whitney, F.A., Crawford, W.R., Harrison, P.J., 2005. Physical processes that enhance nutrient transport and primary productivity in the coastal and open ocean of the subarctic NE Pacific. Deep-Sea Research II 52, 681–706.

Wroblewski, J.S., 1977. A model of phytoplankton plume formation during variable Oregon upwelling. Journal of Marine Research 35, 357–394.